



HelioSwarm: A Multipoint, Multiscale Mission to Characterize Turbulence

Kristopher G. Klein¹ · Harlan Spence² · Olga Alexandrova³ · Matthew Argall² · Lev Arzamasskiy⁴ · Jay Bookbinder⁵ · Theodore Broeren¹ · Damiano Caprioli⁶ · Anthony Case⁷ · Benjamin Chandran² · Li-Jen Chen⁸ · Ivan Dors² · Jonathan Eastwood⁹ · Colin Forsyth¹⁰ · Antoinette Galvin² · Vincent Genot¹¹ · Jasper Halekas¹² · Michael Hesse⁵ · Butler Hine⁵ · Tim Horbury⁹ · Lan Jian⁸ · Justin Kasper⁷ · Matthieu Kretzschmar¹³ · Matthew Kunz¹⁴ · Benoit Lavraud^{11,15} · Olivier Le Contel¹⁶ · Alfred Mallet¹⁷ · Bennett Maruca¹⁸ · William Matthaeus¹⁸ · Jonathan Niehof² · Helen O'Brien⁹ · Christopher Owen¹⁰ · Alessandro Retino¹⁶ · Christopher Reynolds¹⁹ · Owen Roberts²⁰ · Alexander Schekochihin²¹ · Ruth Skoug²² · Charles Smith² · Sonya Smith² · John Steinberg²² · Michael Stevens²³ · Adam Szabo⁸ · Jason TenBarge¹⁴ · Roy Torbert⁴ · Bernard Vasquez⁴ · Daniel Verscharen¹⁰ · Phyllis Whittlesey¹⁷ · Brittany Wickizer⁵ · Gary Zank²⁴ · Ellen Zweibel²⁵

Received: 15 April 2023 / Accepted: 14 October 2023
© The Author(s) 2023

Abstract

HelioSwarm (HS) is a NASA Medium-Class Explorer mission of the Heliophysics Division designed to explore the dynamic three-dimensional mechanisms controlling the physics of plasma turbulence, a ubiquitous process occurring in the heliosphere and in plasmas throughout the universe. This will be accomplished by making simultaneous measurements at nine spacecraft with separations spanning magnetohydrodynamic and sub-ion spatial scales in a variety of near-Earth plasmas. In this paper, we describe the scientific background for the HS investigation, the mission goals and objectives, the observatory reference trajectory and instrumentation implementation before the start of Phase B. Through multipoint, multiscale measurements, HS promises to reveal how energy is transferred across scales and boundaries in plasmas throughout the universe.

Keywords Turbulence · Space plasma · Heliophysics · NASA mission · HelioSwarm

1 Introduction

Turbulence is multiscale disorder. It is the process by which energy that has been injected into a system is transported between fluctuating magnetic fields and plasma motion with

Note by the Editor: This is a Special Communication. In addition to invited review papers and topical collections, Space Science Reviews publishes unsolicited Special Communications. These are papers linked to an earlier topical volume/collection, report-type papers, or timely papers dealing with a strong space-science-technology combination (such papers summarize the science and technology of an instrument or mission in one paper).

Extended author information available on the last page of the article

larger and smaller spatial scales. Once this cascade of energy reaches sufficiently small scales, dissipation mechanisms can act efficiently to remove energy from the fluctuations, leading to heating of the constituent particles. Detailed reviews of models and observations of plasma turbulence can be found in Alexandrova et al. (2013), Bruno and Carbone (2013), Kiyani et al. (2015), Matthaeus (2021), Schekochihin (2022). Observations from single spacecraft provide only information along a single path through a turbulent system; leveraging such measurements to understand turbulence relies on assumptions about the underlying spatial and temporal structure (Taylor 1938; Fredricks and Coroniti 1976). Clusters of four spacecraft provide more information about spatial structure, but are sensitive to only a single scale for a given configuration (Paschmann and Daly 1998, 2008). Understanding fundamental processes such as turbulence requires characterizing the underlying fluctuations and their dynamic evolution across many characteristic scales simultaneously. HelioSwarm (HS) is a Heliophysics Division NASA Medium-Class Explorer mission designed to make such multiscale observations.

HS, currently in Phase B-prep, is the first mission that will make the required measurements to transform the current understanding of space plasma turbulence, using a first-ever swarm of nine spacecraft (SC), composed of one *Hub* and eight *Nodes*. The nine spacecraft, comprising the *HelioSwarm Observatory*, co-orbit in a lunar resonant Earth orbit, with a 2-week period, a mean-apogee radius of $\sim 60R_E$ and a mean-perigee radius of $\sim 11R_E$, where $R_E = 6.371 \times 10^6$ m is the Earth's radius. This orbit, illustrated in Fig. 1, enables measurements of a variety of near-Earth plasma environments, including the pristine solar wind (SW), the magnetically connected foreshock, the magnetosheath, and the magnetosphere. Carefully designed trajectories produce separations between the spacecraft spanning magnetohydrodynamic (MHD) and sub-ion (e.g., ion gyroradius) spatial scales, allowing us to address a broad set of questions about the three-dimensional dynamics of magnetized turbulence. Answering these open questions was identified as a science priority in the 2013 Heliophysics Decadal Survey (Council 2013) and is deeply rooted in decades-earlier recommendations by the space science community in the 1980 report by the Plasma Turbulence Explorer Study Group (Montgomery et al. 1980) and work done in preparation for the Cross-Scale mission concept (Schwartz et al. 2009). As the first multipoint, multiscale mission, HS gives an unprecedented view into the nature of space plasma turbulence.

In Sect. 2, we describe the scientific motivation for HS and in Sect. 3 we enumerate the specific mission goals and objectives. Sections 4 and 5 describe the requirements on what the missions will measure and the observatory trajectories and instrumentation. Section 6 illustrates the application of analysis methods to synthetic data modeling future observations drawn from numerical simulations of turbulence. Conclusions and ongoing work towards the scheduled launch date at the end of this decade are discussed in Sect. 7.

2 Scientific Background and Motivation

Turbulent systems consist of fluctuations spanning a wide range of spatial and temporal scales. Fluctuations interact nonlinearly, typically with a net transfer of energy from larger to smaller spatial scales. This process, the energy cascade, couples the *injection* range of scales, through a lossless *inertial* range, into a *dissipation* range where heating occurs. Turbulence in plasmas is significantly more complex than in hydrodynamics: plasma motion couples to dynamically significant electromagnetic fields, the system possesses many characteristic spatial and temporal scales, supports many different waves and fluctuations, and in weakly collisional systems many mechanisms other than viscosity can act to dissipate

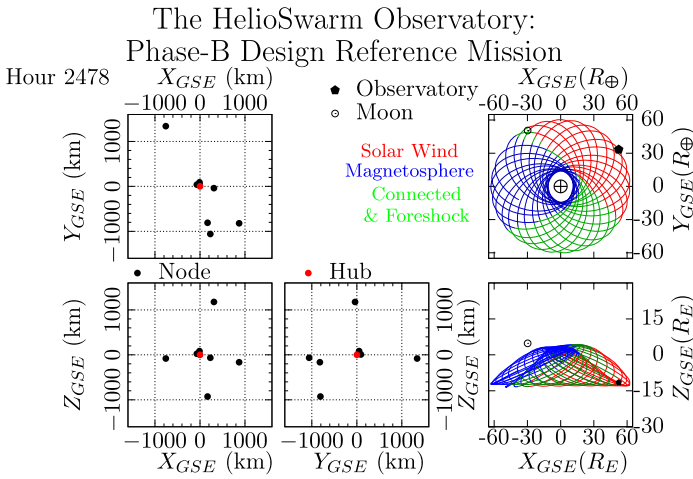


Fig. 1 HelioSwarm Observatory Configuration drawn from the Phase B Design Reference Mission (DRM) trajectory. In the right row, the Observatory location (black pentagon) and orbits relative to Earth over the 12-month Science Phase are shown in both the X-Y and X-Z GSE planes. Lunar position is indicated by an open circle for reference, with different regions of near-Earth plasmas indicated with color, as described in Sect. 4.6. The remaining panels characterize two-dimensional projections of the relative configurations of the eight Nodes (black) with respect to the central Hub (red) in Geocentric Solar Ecliptic (GSE) coordinates. A video of the HS DRM Configuration throughout the Science Phase is available in Online Resource

the cascade. Additional details on the current state of plasma turbulence research can be found in recent reviews, e.g. Bruno and Carbone (2013), Kiyani et al. (2015), Verscharen et al. (2019). The most energetic SW fluctuations are non-compressive (Alexandrova et al. 2008) with properties resembling Alfvén waves (Belcher and Davis 1971; Matthaeus et al. 1999; Howes 2015). Different types of fluctuations nonlinearly interact in different ways (Zank et al. 1996; Matthaeus et al. 1999; Schekochihin et al. 2009; Kunz et al. 2015, 2018) resulting in dramatically different outcomes. The ubiquity of turbulence in space and astrophysical plasmas makes it a leading candidate for the process governing the thermodynamics of a wide range of systems. For instance, turbulence is conjectured to enable angular momentum transport in accretion disks (Balbus and Hawley 1998), amplify galactic magnetic fields (Kulsrud and Zweibel 2008), affect transport processes (Kunz et al. 2022) and establish high temperatures in the intracluster medium of galaxy clusters (Zhuravleva et al. 2018), determine the dispersal and mixing of elements in the Interstellar Medium (ISM) (Scalo and Elmegreen 2004), and play a key role in star formation (McKee and Ostriker 2007).

SW turbulence at the injection scales, where the spectrum steepens from an observed f^{-1} power law (Smith et al. 1995; Matthaeus et al. 2007), has been hypothesized to be driven by large-scale structures. Recent observations from Parker Solar Probe (PSP) indicate that this regime is formed due to SW processing in the near-Sun environment (Huang et al. 2023; Davis et al. 2023). Measurements of the scale-to-scale rate of energy transfer, the cascade rate, near the end of the injection range generally agree with rates near the start of the inertial range, as has been explicitly demonstrated in different kinds of space plasmas using both Magnetospheric Multiscale (MMS) (Bandyopadhyay et al. 2018) and PSP (Bandyopadhyay et al. 2020) observations.

Inertial-range observations (Matthaeus and Goldstein 1982) exhibit scale-invariant energy transfer consistent with Kolmogorov theory (Kolmogorov 1941, 1962): turbulent structures splitting into ever-smaller fluctuations while conserving energy. The inertial range

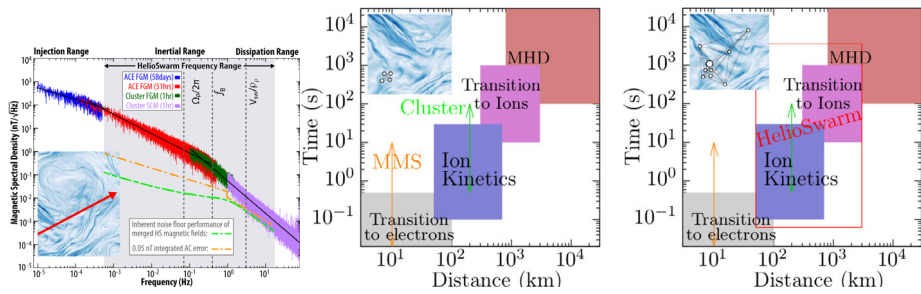


Fig. 2 Single spacecraft missions only provide statistical properties of SW turbulence averaged over both long times and different kinds of turbulence. This approach relies on Taylor's hypothesis to map observed time series to advected structures, measuring only a single 1D slice of the turbulence (red line in inset) and thus only provides a crude measure of turbulent properties. Previous multipoint missions, e.g. MMS and Cluster, are only able to characterize spatial structure at a single-scale. The HS observatory will encompass MHD and ion scales simultaneously, enabling the characterization of multiscale structure and dynamics of turbulence in near-Earth plasmas. Adapted from Verscharen et al. (2019) and Arzamasskiy et al. (2019)

plasma behaves like a MHD fluid (Davidson 2001), with MHD turbulence theory describing relevant phenomena in space physics and astrophysics (Moffatt and Dormy 2019; Parker 1979; Kulsrud 2005) and predicting some SW features (Matthaeus and Velli 2011; Horbury et al. 2012; Verscharen et al. 2019). For example, Fig. 2 shows a composite interplanetary magnetic field (IMF) power spectrum from three magnetometers at 1 AU measured over different time intervals from tens of days to an hour as the SW rapidly sweeps past the spacecraft.

MHD theory adequately describes the inertial range spectral slope, but provides no guidance in the critical higher-frequency transition connecting inertial and dissipation ranges, which begins near the proton gyrofrequency $f_p \equiv \Omega_p/2\pi$. At observed frequencies of about $f_{\text{break}} \sim 0.33$ Hz in the SW at 1 AU—approximately equivalent to advected length scales of $L_{\text{break}} = v_{\text{SW}}/f_{\text{break}} \sim 1200$ km for typical solar wind speeds, the inertial range scale-invariance ends. This break arises before sub-ion scales (e.g., ion gyroradius, ρ_p), typically at apparent frequencies of $v_{\text{SW}}/\rho_p \sim 3$ Hz (length scales ~ 100 km) (Klein and Vech 2019). Other characteristic turbulence scales derived from hydrodynamic turbulence theory, such as the Taylor microscale (Taylor 1935), have been constrained by observations in the solar wind to have sizes on the order of 1000's of km (Weygand et al. 2009; Matthaeus et al. 2005; Bandyopadhyay et al. 2020a).

In Fig. 2 this breakdown is seen as a change in spectral slope at the transition between inertial and dissipation ranges. The spectral break suggests a change in the dominant physical processes and a loss of cascaded energy. The energy removed from the cascade will be converted into charged particle heating and acceleration. All proton damping of turbulent fluctuations occurs at proton-kinetic scales. The remainder of the energy cascaded to smaller scales will be available to heat the electrons.

This process of turbulent dissipation is why SW plasma is much hotter than simple theories of adiabatic expansion would predict (Marsch 2012). If the SW were an adiabatically expanding ideal gas, the protons at Earth would be much cooler than observed (Smith et al. 1995) and protons at Jupiter orbit (~ 5 AU) would be 8 times cooler than at 1 AU, in contrast to Voyager observations (Richardson et al. 1995). Non-adiabatic heating via turbulence dominates plasma thermodynamics throughout much of the solar system, and is a leading candidate for accelerating the SW (Cranmer and van Ballegoijen 2012; Verdini et al. 2010).

The exact heating mechanisms leading to this heating are a matter of substantial debate. Determining the nature of these mechanisms requires observing 3D distributions of the turbulent fluctuations. Plasma turbulence is inherently anisotropic due to preferred directions associated with the IMF (Boldyrev 2006; Schekochihin et al. 2009), radial expansion (Woodham et al. 2021) and large-scale gradients (Völk and Alpers 1972; Grappin et al. 1993; Greco et al. 2012). If turbulent fluctuations vary primarily parallel to the IMF (slab-like) (Ghosh et al. 1998), then non-compressive, Alfvénic fluctuations would, at small scales, ultimately dissipate energy via ion-cyclotron wave (ICW) heating (Kasper et al. 2013). However, for fluctuations that vary mostly perpendicular to the IMF (quasi-2D (Matthaeus et al. 1990) or “critically balanced” (Mallet et al. 2015) with $k_{\perp} \gg k_{\parallel}$), ICW heating is exceedingly weak. In this regime, dissipation instead occurs via other mechanisms such as Landau damping (TenBarge and Howes 2013) or stochastic heating (Chandran et al. 2010). Recent work on imbalanced cascades, the so-called *helicity barrier* (Meyrand et al. 2021; Squire et al. 2022) complicates these models by providing a pathway for low-frequency, anisotropic turbulence fluctuations to develop ion-scale structure parallel to the magnetic field, enabling dissipation via ICWs. If turbulent structures are highly anisotropic sheets, they may undergo magnetic reconnection (Matthaeus and Lamkin 1986; Mallet et al. 2017; Loureiro and Boldyrev 2017) interrupting the cascade and inducing heating and particle acceleration, hints of which have been seen in observations (Vech et al. 2018) and numerical simulations (Dong et al. 2022). Other observations and simulations provide evidence that heating is intermittent and associated with current sheet-like structures (e.g. Greco et al. 2010; Wu et al. 2013; Wan et al. 2016) or magnetic vortices or solitons (e.g. Perrone et al. 2016; Lion et al. 2016; Roberts et al. 2016; Wang et al. 2019). To distinguish among these requires an accurate determination of the 3D power distribution. Previous determinations using single spacecraft use long time series for sufficient statistics, (Horbury et al. 2012; Chen et al. 2011, 2012; Chen 2016), combining together intervals of turbulence with very different properties. The regulation of energetic particle transport, in both SW (Jokipii 1972) and astrophysical plasmas (Zweibel 2013), is also sensitive to the turbulence spectrum and its anisotropies.

At a fundamental level, the nature of turbulent fluctuations in magnetized plasmas remains unknown: is it an MHD extension of hydrodynamic eddies (Matthaeus and Velli 2011), a quasi-2D system (Zank and Matthaeus 1992), critically balanced wave-like fluctuations (Schekochihin et al. 2009; Mallet et al. 2015), or a dynamically evolving mixture? The complexity of plasma turbulence precludes simple, analytic solutions. Numerical simulations are invaluable but limited by incomplete physics and small system size (Parashar et al. 2015). Confined laboratory plasmas (Brown and Schaffner 2015; Forest et al. 2015; Gekelman et al. 2016) have similarly limited scale separations and access to SW-like physical parameters.

The SW is a natural laboratory where we can finally answer these questions by concurrently observing turbulent energy transfer and ion heating over a targeted range of scales. However, single-spacecraft observations of SW turbulence are fundamentally limited. Multi-spacecraft missions enabled advances by creating geometric configurations to sample single-scale plasma structure without relying on Taylor’s hypothesis (further discussed in Sect. 3.1.1). Four- (Cluster (Escoubet et al. 2001), MMS (Burch et al. 2016)) and five-spacecraft (Time History of Events and Macroscale Interactions during Substorms (THEMIS) (Angelopoulos 2008)) missions produce configurations that allow for single-scale measurements (Chen et al. 2019; Escoubet et al. 2021). While these missions have provided significant insights to dynamics at a particular scale, e.g. studies of electron processes enabled by MMS (Burch and Hwang 2021), they do not enable a simultaneous characterization of the larger three-dimensional turbulent structures in which they are embedded.

Even with advanced analysis techniques, scales sampled using four spacecraft cover at most a factor of ~ 10 , as demonstrated for instance with the wave-telescope technique (Sahraoui et al. 2010a,b), nowhere near the > 2 orders of magnitude necessary to simultaneously measure across inertial and ion dissipation ranges. That many more than four spacecraft will be necessary for studying these multiscale processes has been recognized by the scientific community for several decades, (e.g. Montgomery et al. 1980), and previous mission concepts such as Cross-Scale (Schwartz et al. 2009) have served as pathfinders for HS. HS's configurations created by 9 spacecraft provide the first simultaneous multiscale view of plasma turbulence, targeting key scales from MHD to sub-ion scales. By measuring plasmas at multiple scales simultaneously, the HS Observatory promises transformative impacts in our understanding of turbulence, which will be a boon for heliophysics, astrophysics, and plasma physics (Armstrong et al. 1981; Elmegreen and Scalo 2004; Mac Low and Ossenkopf 2000).

3 HelioSwarm Goals and Objectives

HS advances Goal 4 of the 2013 National Academy of Sciences (NAS) Heliophysics Decadal Survey (Council 2013) (DS) which calls on the community to “[d]iscover and characterize fundamental processes that occur both within the heliosphere and throughout the universe.” Magnetized plasma turbulence is the primary mechanism responsible for transforming energy injected at largest scales into small-scale motions, eventually dissipating as plasma heat. Plasma turbulence is universal, responsible for energy transfer in such diverse systems as the solar corona, SW, pulsar wind nebulae, accretion discs, interstellar medium, planet formation regions, and laboratory fusion devices. Only the SW is both of sufficient size for multiscale observations and accessible for *in situ* measurements. Turbulence is identified as one of eight DS Goals for SW/Magnetosphere Interactions (SWMI): “Understand the origins and effects of turbulence and wave particle interactions.” Because of that importance, turbulence is also identified as a SWMI Decadal Imperative: “Implement...a multi-spacecraft mission to address cross-scale plasma physics.” Likewise, the NASA Heliophysics Roadmap (NASA 2014) highlights “Understand[ing] the role of turbulence and waves in the transport of mass, momentum, and energy” as one of its key Research Focus Areas of high priority. Long standing heliophysics mysteries — such as how the solar coronal temperature increases by orders of magnitude and how the SW is accelerated and heated — remain unanswered after decades of research because we lack detailed understanding of how energy in turbulent plasmas heat particles. HS advances these NAS and NASA science priorities, and will specifically resolve six science objectives (O) associated with two overarching science goals (G).

- **(G1)** Reveal the 3D spatial structure and dynamics of turbulence in a weakly collisional plasma.
 - *G1O1* Reveal how turbulence energy transfers in the typical SW plasma as a function of scale and time.
 - *G1O2* Reveal how the turbulent cascade of energy varies with background parameters in different SW environments.
 - *G1O3* Quantify the transfer of turbulent energy between fields, flows, and proton heat.
 - *G1O4* Identify the thermodynamic impacts of intermittent structures on protons.
- **(G2)** Ascertain the mutual impacts of turbulence, variability, and boundaries near large scale structures.
 - *G2O1* Determine how SW turbulence affects and is affected by large-scale structures such as Coronal Mass Ejections (CMEs) and Corotating Interaction Regions (CIRs).

- *G2O2* Determine how driven turbulence differs from that in undisturbed SW.

The HS goals and objectives in turn define the observatory and instrument requirements, detailed in Sects. 4 and 5.

3.1 G1: Reveal the 3D Spatial Structure and Dynamics of Turbulence in a Weakly Collisional Plasma

Most of our limited present understanding of turbulence is based on single point observations. Clusters of four spacecraft provide improvements by exploring processes occurring at a single size scale at a single time. As any three points define a plane, extraction of non-coplanar 3D information (such as curls or gradients) requires four points and appropriate analysis methods (Paschmann and Daly 1998, 2008). However, turbulence is fundamentally multiscale; HS for the first time simultaneously explores the dynamics of processes at multiple size scales.

3.1.1 G1O1: Reveal How Turbulent Energy Transfers in the Typical SW Plasma as a Function of Scale and Time

Using the undisturbed SW as a natural laboratory, with typical plasma parameters, HS measures fluctuations in the plasma velocity and density ($\delta\mathbf{v}$ and δn) and magnetic field ($\delta\mathbf{B}$) at MHD to sub-ion scales simultaneously using the instrument suite described in Sect. 5. These data reveal how turbulent energy is distributed and transferred as a function of space and time. Turbulent fluctuations are affected by local magnetic fields (Iroshnikov 1963; Kraichnan 1965; Schekochihin et al. 2009; Matthaeus et al. 1990), so we must characterize SW turbulence relative to the local IMF direction. Such studies have been performed with data from single spacecraft; c.f. the review in Chen (2016), and necessarily rely upon the assumption of essentially frozen turbulence structures, an approximation known as the Taylor hypothesis (Taylor 1938; Fredricks and Coroniti 1976; Osman and Horbury 2007; Klein et al. 2014) that neglects temporal variations and can infer only 1D variation along the SW flow direction. These studies also frequently assume that the turbulence is insensitive to the angle between the SW velocity and the magnetic field, using variations in θ_{vB} to study the functional dependence of the turbulence on the angle between the wavevector and magnetic field θ_{kB} . Recent work (Woodham et al. 2021) suggests that this assumption may not be valid; verifying this claim will require sampling the turbulent structures both along and transverse to the magnetic field direction simultaneously, a measurement that HS is designed to produce.

With HS, the Taylor hypothesis can be directly evaluated. Spectral information is also available from proven analysis techniques (Sect. 6) such as 2-point correlations, structure functions, space-time correlations, and cascade rate analysis (Matthaeus and Goldstein 1982; Horbury et al. 2012; Matthaeus et al. 1990; Hamilton et al. 2008; Chen et al. 2011; Horbury et al. 2008; Mallet et al. 2016), from which it is possible to extract information about 3D spectral structure (Osman et al. 2011; Hamilton et al. 2008; Bieber et al. 1996) and its intrinsic, scale-dependent decorrelation times. These techniques frequently use measurements of the velocity and magnetic fields directly, or the Elsasser variables ($\mathbf{z}^{\pm} = \delta\mathbf{v} \pm \delta\mathbf{b}$) (Elsasser 1950) in which the magnetic field is expressed in Alfvén (velocity) units ($\delta\mathbf{b} = \delta\mathbf{B}/\sqrt{\mu_0 n_p m_p}$) and δ indicates the use of a fluctuating quantity.

A prominent example of the use of Elsasser variables is the MHD 3rd-order law

$$\nabla \cdot \langle \Delta \mathbf{z}^{\mp} | \Delta \mathbf{z}^{\pm} |^2 \rangle = -4\epsilon^{\pm}, \quad (1)$$

an analytic result involving spatial increments $\Delta \mathbf{x}$ of the Elsasser fields $\Delta \mathbf{z}^{\pm} = \mathbf{z}^{\pm}(\mathbf{x} + \Delta \mathbf{x}) - \mathbf{z}^{\pm}(\mathbf{x})$, and $\langle \dots \rangle$ denotes ensemble average. This relation can be used to determine the energy cascade rate associated with the forward and backward Elsasser fields ϵ^{\pm} (Osman et al. 2011). Formally, this requires knowledge of 3D anisotropies. Previous studies have usually made assumptions about isotropy (MacBride et al. 2005, 2008; Stawarz et al. 2009; Coburn et al. 2012; Hadid et al. 2017) or only measured ϵ over limited range of scales (Bandyopadhyay et al. 2018). HS can implement the isotropic form at all nine spacecraft, but also can integrate the 3D form of the 3rd-order law at several scales simultaneously, making use of all 36 spacecraft pairs to compute the 2-point spatial increments. HS provides simultaneous 3D multipoint knowledge needed to infer spatial gradients contained in the 3rd-order equation, quantifying directly those key terms for the first time, bypassing simplifying assumptions about isotropy, to measure cross-scale energy transfer rates definitively.

No comprehensive observational evidence exists to distinguish between proposed theories of turbulent energy transfer. A review of such theories can be found in NAS 2020 Plasma Decadal Panel white papers (Klein et al. 2019; Matthaeus et al. 2019; TenBarge et al. 2019) and other reviews (Schekochihin et al. 2009; Oughton et al. 2017). Candidate energy transfer processes are related to relevant dynamical timescales that include wave propagation, random and coherent sweeping of small structures by larger structures, and nonlinear wave distortion (Orszag and Patterson 1972; Tennekes 1975; Nelkin and Tabor 1990; Sanada and Shanmugasundaram 1992; Servidio et al. 2011). Numerical simulations provide insights regarding which of these are important but results remain inconclusive due to fundamental limitations associated with the necessary trade offs between the volume of space simulated and the physical processes included in the equations evolved. HS provides observations to distinguish and refine our understanding of the relevance of these processes.

3.1.2 G102: Reveal How Turbulent Cascade of Energy Varies with Background Parameters in Different SW Environments

Turbulence and plasma conditions in fast and slow SW differ systematically in terms of density, temperature anisotropy, and collisional age (Belcher and Davis 1971; Dasso et al. 2005; MacBride et al. 2005, 2008; Borovsky et al. 2019; Kasper et al. 2008). Slow SW turbulence is more highly variable in nature than the fast SW (Dasso et al. 2005) and due to its longer transit from the Sun, has more time to evolve toward a fully developed state. These differences have been assessed in limited fashion with single-point ((Breech et al. 2008; Vech et al. 2017), e.g., Wind, Voyager) and single-scale (Bandyopadhyay et al. 2018) (e.g., MMS) measurements. The varying SW speed is also associated with variations in proton number density, temperature, alpha particle density, and IMF strength. Plasma $\beta = 8\pi n k_b T / B^2$, the ratio of thermal to magnetic pressure, a particularly important regulator of plasma processes (Chen et al. 2014), and power imbalances (such as cross helicity σ_C and residual energy σ_R , (Wicks et al. 2013)), are also highly variable in the SW. These parameters influence the underlying energy cascade from MHD to sub-ion scales. HS targets to study the impact of this variability on the dynamics of the turbulence.

3.1.3 G103: Quantify Transfer of Turbulent Energy Between Fields, Flows, and Proton Heat

Dissipation of turbulence is one of the most important factors influencing heating and particle energization in the universe. Consequently, our goal of investigating energy transfer must include how the cascade heats protons. Protons are of primary importance as they are

the dominant species in terms of both mass and momentum. How and how much energy is delivered to protons via dissipation processes determines the overall partitioning of energy across all species. Primary candidate mechanisms include: ICWs and cyclotron resonances (Hollweg and Isenberg 2002); Landau damping (TenBarge and Howes 2013); stochastic heating by large amplitude turbulent fluctuations (Chandran et al. 2010); and energization through intermittent structures, including magnetic reconnection (Dmitruk et al. 2004) and trapping in secondary magnetic islands (Ambrosiano et al. 1988).

Current observations do not provide clarity. For example, intense ICWs are commonly observed during times when plasma instabilities are present (Gary et al. 2016) in extended “storms” during quiet SW and radial IMF (Jian et al. 2014). Because ICWs are capable of substantial heating of SW ions, it is important to understand exactly how often they occur. ICWs may be omnipresent but can only be detected by a single spacecraft when the SW flow is aligned with the local IMF (i.e., radial field configurations). Applying methods such as the wave telescope technique to HS observations, Sect. 6, will identify ICWs when the IMF is not radial, thus establishing definitively whether ICWs are always present or not.

The various spatial regions that HS will be measuring, in particular the foreshock (e.g. see review in (Eastwood et al. 2005)), are excellent natural laboratories for studying plasma waves at a variety of frequencies, as well as understanding the mechanisms by which such waves are created and subsequently interact with the local turbulence. HS will provide insight not only into the basic processes, but also shed light on the role of inhomogeneity and gradients in the background plasma properties, as well as the non-linear evolution.

All aforementioned mechanisms occur at ion time and length scales and create characteristic signatures in underlying proton velocity distribution functions (VDFs); each mechanism deposits differing fractions of energy to the protons (Chandran et al. 2010; He et al. 2015; Matthaeus et al. 2016a). The absence or presence of these signatures reveals which dissipation pathways operate; their relative strengths quantify their relative importance. Measurements of proton temperature at ion heating time scales allows HS to quantify proton heating directly. One analysis method, colloquially referred to as ‘PiD’, makes use of the measured pressure tensor Π_{ij} and flow gradients $S_{ij} = \nabla_i \mathbf{u}_j$ to compute the full pressure-strain interactions $\Pi : S$ which is the rate of production of proton internal energy (Yang et al. 2019). These methods are enabled in HS by simultaneous measurement of proton distribution functions and 3D multiscale turbulence, a combined capability lacking in all previous missions. HS will allow us to directly quantify relationships between the distribution of turbulence fluctuations and transformation into proton heat.

3.1.4 G104: Identify Thermodynamic Impacts of Intermittent Structures on Protons

Intermittency is a universal property of turbulence in which dissipation processes concentrate into small fractions of available volumes (Horbury and Balogh 1997; Matthaeus et al. 2015), giving rise to current sheet and other intermittent coherent structures, e.g. Alfvénic vortices (Alexandrova 2008; Perrone et al. 2016; Lion et al. 2016). Such structures, which have been studied in numerical simulations (Karimabadi et al. 2013; Grošelj et al. 2019) and *in situ* observations (Osman et al. 2011), alter the dynamics of turbulent plasmas, dramatically impacting how turbulence heats plasma (Mallet et al. 2019). Indeed, magnetic reconnection of turbulently generated current sheets has been predicted to arise (Matthaeus and Lamkin 1986; Mallet et al. 2017; Loureiro and Boldyrev 2017), interrupting the cascade and driving heating and particle acceleration. Solar wind observations and numerical simulations, (e.g. Greco et al. 2010; Wu et al. 2013; Wan et al. 2016) provide evidence that heating is intermittent and associated with current sheet-like structures. The introduction of

Grošelj et al. (2019) provides an overview of recent numerical and observational findings on the characteristics and behaviors of these intermittent structures. Recent studies from MMS show that HS is expected to observe turbulent reconnection, most probably in the flank magnetosheath (e.g. Stawarz et al. 2022). Such observations will allow the evolution and properties of turbulent reconnection to be studied in detail, in particular the volume filling of reconnection sites, the nature of energy exchange, and quantifying the spatio-temporal scales on which ion coupling to turbulent reconnection occurs.

Cluster and MMS pioneered the ability to resolve thin structures with 4-point curlometer and gradient techniques (Dunlop et al. 2002a,b). While revolutionary, such techniques probe only a single scale at a time. HS provides combinatorically more spacecraft groupings and simultaneous access to multiple scales, tremendously expanding 3D anisotropic measures of intermittency with well-developed analysis tools, as described in Sect. 6.

By measuring intermittency of turbulent fluctuations at inertial and ion scales simultaneously, HS differentiates between models of nonlinear coupling, that predict enhanced amplitudes of Elsasser fluctuations δz at small scales compared to a scale-independent normal distribution of amplitudes. HS also resolves the intermediate scales to provide further differentiation.

3.2 G2: Ascertain the Mutual Impacts of Turbulence, Variability, and Boundaries Near Large Scale Structures

While undisturbed SW is a pristine environment, disturbed SW occurs from impacts of either large scale structures of solar or heliospheric origin or Earth's magnetosphere and provides different environments to explore. Impacts are mutual: turbulence can impact large-scale structures and boundaries and those same structures can in turn change the nature of turbulence. Goal Two focuses on these mutual interactions.

3.2.1 G201: Determine How SW Turbulence Affects and Is Affected by Large-Scale Structures Such as CMEs and CIRs

Passage of interplanetary coronal mass ejections (CMEs) (Jian et al. 2018) or corotating interaction regions (CIRs) (Goldstein et al. 1984; Jian et al. 2019) disturb the SW from its pristine state. These large-scale features re-inject energy and thus modify SW turbulence. While turbulence levels are reduced within CME structures, HS enables 3D characterization of this (possibly weak) low-plasma β turbulence contained within a large scale force-free structure. Near CMEs, driven turbulence departs significantly from that of the pristine SW; HS will diagnose 3D turbulence modifications associated with diffusive shock acceleration (le Roux et al. 2015) near fast CMEs and waves driven by the CME's propagation (Zhao et al. 2021). Passage of both CMEs and CIRs through pristine SW turbulence allows us to explore differences in these environments, enabling us to determine when and how specific energy transfer and heating processes become important.

3.2.2 G202: Determine How Driven Turbulence Differs from That in Undisturbed SW

The terrestrial bow shock, foreshock, and magnetosheath are permeated with magnetic and plasma fluctuations, strongly driving and modifying the turbulent spectrum across inertial and dissipation scales both in amplitude and shape (Chen et al. 2019). These regions represent parameter regimes not accessible in pristine SW. The dynamics in these locations are

significantly different; for example, ions reflected off the bow shock can lead to the self-generation of turbulence, which takes the form of non-linear wave penetrating into the inner magnetosphere (Takahashi et al. 2016), while at the shock, turbulence generates high-speed jets that regularly impact the magnetopause, resulting in dayside reconnection (Hietala et al. 2018). Turbulence is also seen to drive magnetic reconnection in these regions (Retinò et al. 2007). Finally, magnetospheric regions can be turbulent (Chasapis et al. 2017, 2020; Bandyopadhyay et al. 2020a,b), but of a different nature (e.g. high plasma beta, compressible, or magnetically dominated) (Maruca et al. 2018). Objective Two explores this variety of accessible systems to compare how driven environments differ from pristine SW.

4 HelioSwarm Observatory Design

The specific design of the HS Observatory is driven by decades of measurements from near-Earth plasmas of characteristic length and time scales as well as derived dimensionless parameters that are predicted to govern the behavior of magnetized turbulence.

4.1 Quantities to Be Measured

As discussed in Sect. 3.1.1, the primitive variables that describe magnetized turbulence at MHD scales are the Elsasser variables (Elsasser 1950) composed of magnetic fields and particle densities and velocities. G1O1 requires measurements of the IMF, SW proton density, and SW velocity. It must do so in undisturbed, most-probable SW for which the range of proton densities is 1.6 to 20 cm^{-3} and magnetic field can be as large as 25 nT, but typically larger than 2.6 nT (at the 90% occurrence rate) (Wilson et al. 2018; Klein and Vech 2019). To resolve at the lowest typical field strength, we require 10% resolution (0.26 nT), corresponding to 0.15 nT per axis. Such measurements allow construction of Elsasser variables, needed for magnetized turbulence analysis at each measurement location.

Measurements of the SW proton density, velocity and IMF must be made at multiple points in 3D encompassing the turbulent cascade during average SW conditions, within large scale structure analysis intervals—equivalent to approximately one hour long continuous observations—at cadences, time knowledge, and sensitivities required to resolve and align SW and IMF variations down to sub-ion scales.

4.2 Spatial Resolution

To measure the multiscale nature of turbulence, HS's baseline separations between the nine spacecraft are designed to simultaneously span MHD scales and ion kinetic scales, enabling the simultaneous resolution of MHD and sub-ion processes and the transition between these scales, exemplified by the observed spectral break (Goldstein et al. 1994; Leamon et al. 1999; Hamilton et al. 2008; Chen et al. 2014; Vech et al. 2017, 2018; Woodham et al. 2018) (see also Fig. 2). Values for these physical dimensions are empirically known from decades of SW observations (Borovsky et al. 2019; Wilson et al. 2018; Woodham et al. 2018; Klein and Vech 2019). Figure 3 shows the joint probability distribution function (PDF) of the proton gyroscale ρ_p and spectral break scale $L_{\text{break}} = v_{\text{sw}}/f_{\text{break}}$. These observations define three ranges: MHD scales at > 1200 km; transition scales between 100 and 1200 km; and sub-ion structures < 100 km. HS's baseline requirements are established to resolve these characteristic scales simultaneously in 85% of the pristine SW, enabling the Observatory to “encompass the turbulent cascade.”

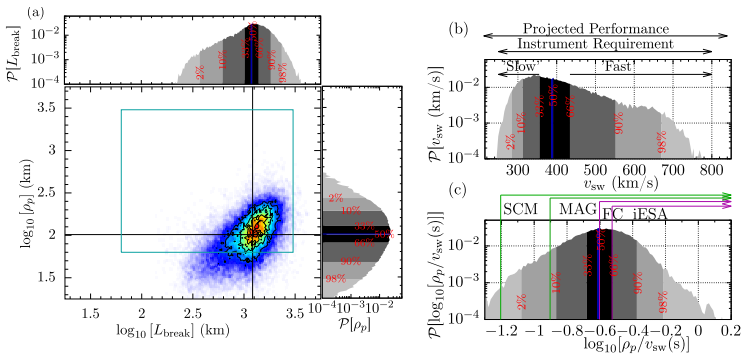


Fig. 3 (a) Joint PDF of proton gyroradius ρ_p and spectral break scale L_{break} as measured by the Wind spacecraft at Earth’s L1 point (Wilson et al. 2018; Klein and Vech 2019). HS’s baseline separations between spacecraft will cover from 3000 km to 50 km (blue box), allowing the observatory to simultaneously measure MHD, transition, and sub-ion physical processes in 85% of the pristine SW. (b) PDF of SW velocity drawn from the same database, compared to FC instrumental requirements and project performance, illustrating that HS will capture both typical and extreme proton velocities. (c) PDF of the advected SW ion timescale ρ_p/v_{sw} , compared to HS instrument cadences, demonstrating that HS will resolve the IMF past ion-scales in nearly all the SW, and resolve both the ion-scale plasma processes in typical SW conditions. In all panels, the red numbers indicate the percentile of the cumulative distribution below the given value

4.3 Temporal Resolution

The Observatory measurement cadence and timing knowledge provide the temporal resolution necessary to resolve advected SW structures. This analysis requires measuring at time cadences from MHD scales down to the sub-ion scales.

Given the observed distribution of SW velocities, see Fig. 3b, we can calculate the ratio of the proton gyroscale ρ_p to v_{sw} to construct an advected proton timescale, Fig. 3c, which plots the observed distribution against instrumental measurement rates. The fluxgate magnetometer (MAG) measures at 16 samples per second (Sps) overlapping with the search-coil magnetometer (SCM, at 32 Sps) providing continuous coverage of larger and/or more slowly advecting structures, while also resolving ion-scale structures traveling at the fastest v_{sw} (~ 800 km/s); The proton density (n) and velocity (v) are measured by Faraday cups (FCs) at a rate of 8 Sps, resolving ion scale structures (~ 100 km) traveling at typical speeds (400 km/s); Measurements of the proton temperature by the ion electrostatic analyzer (iESA) provide the necessary context for the kind of turbulence HS is embedded in, with sufficient temporal resolution to resolve changes in proton velocity distributions to help determine the energy transfer processes associated with ion scale structure.

In order to resolve characteristic SW wave propagation directions across multiple points, HS requires post-facto, relative pairwise separation knowledge of 10% the separation distances. Timing requirements are driven by applying analysis methods described in Sect. 6 to synthetic data combined with models for temporal uncertainty.

4.4 Observatory Stability

Simultaneous statistical analysis of turbulence (e.g. Sect. 6.1) requires not only separations spanning the previous described spatial scales but also samples taken over long enough periods of time to capture the nonlinear reshaping of the underlying structures. One can

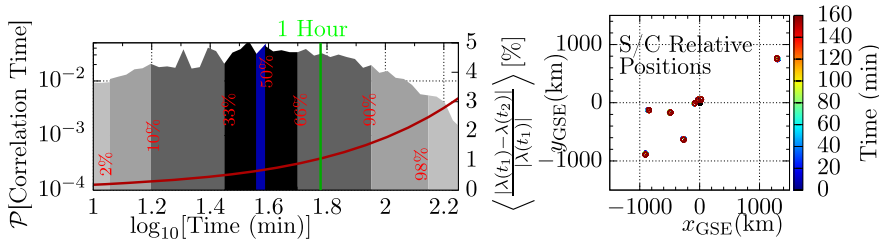


Fig. 4 PDF of correlation time measured by ACE (left panel) (Isaacs et al. 2015) compared to the average change in HS DRM baseline separation magnitudes as a function of time (red line). At right, the $x_{\text{GSE}} - y_{\text{GSE}}$ projection of the evolving Node positions relative to the Hub, with color indicating time since apogee; the significant overlap in positions illustrate the relative stability of the observatory configuration

Table 1 Number of baselines, tetrahedral, and polyhedral (with at least four vertices) configurations that can be constructed from N Spacecraft

# Spacecraft	4	5	6	7	8	9	10	11
Baselines	6	10	15	21	28	36	45	55
Tetrahedra	1	5	15	35	70	126	210	330
Polyhedra	1	6	22	64	163	382	848	1816

calculate the correlation time scale τ by determining the time lag necessary to reduce an autocorrelation of some measured quantity F by $1/e$ from its zero-lag value

$$A[F(t), F(t + \tau)] = \langle F(t)F(t + \tau) \rangle = \langle F(t)F(t) \rangle / e, \tag{2}$$

where $\langle \dots \rangle$ denotes an appropriate ensemble average. Analysis performed on intervals measured within a correlation time are effectively sampling the same population of turbulent fluctuations, and thus can be combined to study the statistical properties of that plasma. Observations of the correlation time scale in the SW (Isaacs et al. 2015; Smith et al. 2018), illustrated in Fig. 4, typically find it ranges from tens of minutes to approximately an hour. This duration of SW data provides robust turbulence analysis yet is short enough to effectively sample the same parcel of SW. These observations drive the timescales over which the observatory spacecraft separations need to be constant, a requirement the HS Design Reference Mission (DRM) satisfies, enabling the accrual of usable intervals for the application of analysis approaches outlined in Sect. 6; the average relative change in the vector baselines increases slowly in time (red line), reaching 0.7% at 60 minutes and 1.5% at 120 minutes.

4.5 Spatial Configurations

In conjunction with spatial separation requirements, the application of the analysis approaches in Sect. 6 require specific spatial configurations. Given N spacecraft, there are $N(N - 1)/2$ distinct pair-wise baseline separations. Similarly, for N spacecraft, one can construct $\binom{N}{4} = \frac{N!}{4!(N-4)!}$ unique tetrahedral configurations, or $\sum_{i=4}^N \binom{N}{i}$ polyhedral configurations with at least four vertices. The number of baselines, tetrahedra, and polyhedra are tabulated as a function of the number of spacecraft in Table 1. The orientation and geometries of these configurations have been carefully tailored so that they span the appropriate size-scales and directions to address the mission objectives, as discussed in the following subsections and illustrated in Fig. 5. Determining when the HS Observatory satisfies these

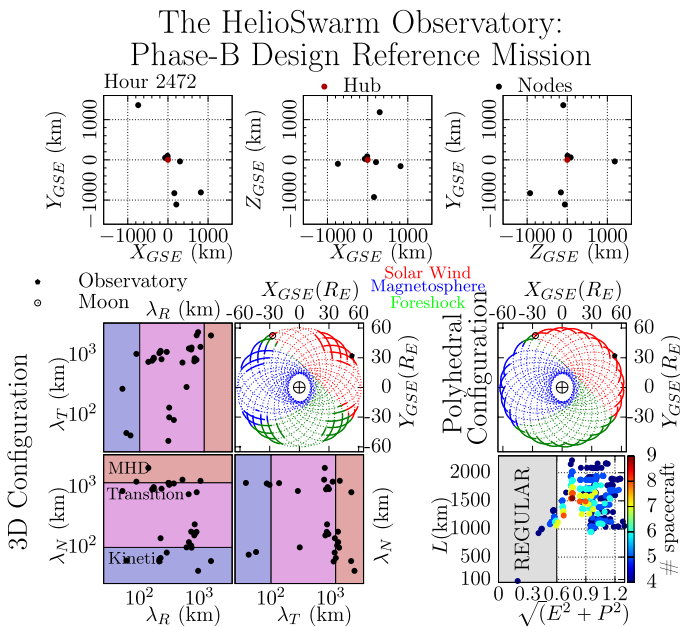


Fig. 5 Summary plot of HelioSwarm Observatory Phase-B DRM positions and separations. *Top Row* Relative positions between the Hub (red) and eight Nodes (black) projected into the GSE coordinate system at hour 2472 from the DRM. *Bottom Left* Projected vector components of the 36 inter-spacecraft baseline separations (black dots) demonstrate coverage of MHD and ion-kinetic scales, as well as the transition region in-between. The lunar resonant orbit of the observatory (black dot) in the GSE coordinate system is shown as colored lines in the upper-right inset, with the moon's location (open circle) included to illustrate scale. Times with orthogonal coverage over all three scales, highlighted with solid lines, arise in the pristine SW (red lines), the magnetically connected SW (green) and the magnetosphere/magnetosheath (blue). *Bottom Right* The size and geometric configurations of the polyhedra constructed by spacecraft subsets of the HelioSwarm observatory. The number of spacecraft is indicated by color, while the size of the polyhedra L and its regularity (the RMS of the elongation E and planarity P) are indicated on the ordinate and abscissa respectively. The times when there are at least two regular polyhedra with characteristic sizes more than a factor of three different are indicated in the upper inset, using the same color scheme as the 3D Configuration inset. As quantified in Table 2, due to the high eccentricity of the orbit, the Observatory samples these regions near apogee for a substantial fraction of the orbit period. A video of the HS DRM Geometries throughout the Science Phase is available in Online Resource 2

configurational requirements is characterized in 1-hour units, during which baseline separations are effectively constant, see Fig. 4. The number of hours satisfying these requirements are laid out in Table 2.

4.5.1 3D Configurations

To calculate cascade rates, correlation scales, and structure functions to characterize the multiscale and 3D nature of turbulence, the 36 unique baselines between HS's nine spacecraft have vector components spanning three orthogonal directions along, transverse, and normal to the Earth-Sun line (Radial, Tangential, Normal (RTN) coordinates) with amplitudes covering MHD, transition, and sub-ion scales, while simultaneously the magnitudes of the baseline vectors also span these three ranges of scales. These *3D configurations*, illustrated in Fig. 5, resolve variations along and across the local magnetic field and flow directions, necessary for verifying theories of anisotropic turbulent transfer and distribution of energy.

Table 2 HS measures thousands of hours in targeted near-Earth regions of space during its 12-month nominal Science Phase, with hundreds of hours in optimal polyhedral (Sect. 4.5.2) and 3D configurations (Sect. 4.5.1) for the application of analysis approaches outlined in Sect. 6, providing measurements to advance the understanding of turbulence in typical (G1O1,G2O2) uncommon (G2O1) and extreme (G1O2) plasma conditions

Phase B DRM; LRD 2028	Fig. 5	Total	3D	Polyhedral
Solar Wind	Red	2881	777	1068
Foreshock	Green	2470	977	852
Magnetosphere/Magnetosheath	Blue	3149	650	639
Science Phase		8850	2404	2559
	Objective	Total	3D	Polyhedral
Pristine SW	G1O1	2015	544	747
Extreme SW	G1O2	58	16	21
SW w/Large Scale Structure	G2O1	546	147	202
Strongly Driven Turbulence	G2O2	5619	1627	1491

4.5.2 Polyhedral Configurations

HS configurations are also designed for multi-point analysis techniques that determine spatial gradients and distributions of power (e.g., wave-telescope, curlometer, and related gradient analysis techniques (Paschmann and Daly 1998, 2008)). Spatial gradient methods require the SC be arranged in a quasi-regular fashion, occupying vertices of pseudo-spherical polyhedra. One can characterize the geometry of these polyhedra by calculating the eigenvectors of the volumetric tensor

$$\underline{\underline{R}} = \frac{1}{N} \sum_{\alpha=1}^N (\mathbf{r}_\alpha - \mathbf{r}_b) (\mathbf{r}_\alpha - \mathbf{r}_b)^T \tag{3}$$

where $\mathbf{r}_b = \frac{1}{N} \sum_{\alpha=1}^N \mathbf{r}_\alpha$ is the mesocenter of the configuration, and \mathbf{r}_α represents the positions of the individual SC. The square roots of the three eigenvalues of $\underline{\underline{R}}$ represent the major, middle, and minor semiaxes of the configuration, a , b , and c . These values can be interpreted directly by defining a characteristic size $L = 2a$, as well as the elongation $E = 1 - \frac{b}{a}$ and planarity $P = 1 - \frac{c}{b}$. Figure 6 illustrates the distribution of polyhedra from a single hour of the HS Observatory configuration. Polyhedra with small elongation E and planarity P , $\sqrt{E^2 + P^2} \leq 0.6$, can be used to accurately measure structure of sizes on the order of the characteristic size L (Sahraoui et al. 2010b; Roberts et al. 2015). HS’s 9 spacecraft produce 382 polyhedra with at least 4 vertices, the minimum needed for 3D analysis techniques, and at many different scales. Additionally, HS has configurations where at least two pseudo-spherical polyhedra exist with at least a 3:1 ratio in L . These formations, referred to as *polyhedral configurations*, simultaneously measure spatial structure of turbulence at multiple scales.

4.5.3 Required Number of Spacecraft

As noted in the Plasma Turbulence Explorer Study Group Report (Montgomery et al. 1980), “A mission aimed at studying turbulence requires simultaneous measurements from N spacecraft... [t]he point at which increasing N by one is not desirable is largely determined by economic considerations.” In selecting nine spacecraft for HS, we have balanced the combinatoric increases in the number of baselines and polyhedra, shown in Table 1, against cost

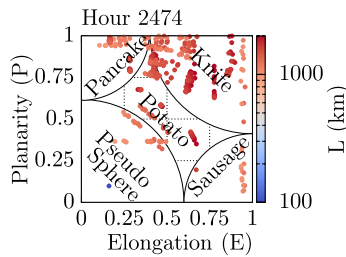


Fig. 6 The distribution of planarity (P), elongation (E), and characteristic size (L, with blue and red representing the smallest and largest scales respectively) of all 382 polyhedra with at least 4 vertices for the HS DRM at an arbitrarily selected hour 2474. The different regions in E-P space are labeled to characterize the geometries of these polyhedra. The Observatory trajectories are designed to have multiple pseudo-spherical polyhedra with significantly different sizes to enable measurements of spatial structures at MHD- and ion-scales simultaneously

and engineering constraints, all while focusing on ensuring that the resulting configurations would be able to measure in three dimensions processes spanning the required MHD, transition, and ion spatial scales simultaneously.

The number of nodes was selected to yield a sufficient number of hours in the two designated spatial configurations defined in Sect. 4.5.1 and 4.5.2 covering the physical scales of interest. For instance, at least seven spacecraft are needed to form two regular tetrahedra spanning significantly separate spatial scales, and the observatory is capable of achieving the required number of configuration hours with seven spacecraft. Nine spacecraft provides redundancy, as discussed in Sect. 4.8, as well as an increase in the rate at which hours with good configurations can be accumulated.

We have additionally performed the analysis techniques described in Sect. 6 using HS-like configurations with arbitrary S/C removed. For most of the statistical analysis methods, such as structure functions or correlation scales, analysis with one or even two fewer measurement points still yields quantitatively similar results, while further reductions to six or fewer spacecraft begin to dramatically limit the spatial scales covered, reducing the ability to resolve in 3D the multiscale phenomena of interest without assumptions about the underlying structures.

4.6 Observatory Orbits

The HS Observatory accesses the near-Earth regions of interest with a 2-week, lunar-resonant, high Earth orbit (HEO) (Plice et al. 2019; Levinson-Muth et al. 2021a,b, 2022). The HS Observatory design and onboard propulsion produce inter-spacecraft separations both along and across the Sun-Earth line. The Nodes perform routine trim maneuvers to maintain customized configurations that satisfy the 3D and Polyhedral requirements over the mission lifetime. Since the science orbit is nearly inertially fixed (with a low rate of apsidal precession), the apogee rotates through the SW, foreshock, and magnetosphere-dominated regions as the Earth completes a single orbit of the Sun. This progression allows the Observatory to sample the pristine SW and regions of strongly driven turbulence during the 12-month Science Phase, addressing both G1 and G2. Details about the design of the orbit can be found in Plice et al. (2019) and Levinson-Muth et al. (2022).

Given an empirical model for the extent of the bow shock (Formisano 1979) and the average orientation of the IMF combined with the phase B DRM trajectories, the HS Observatory spends thousands of hours in the required near-Earth regions of interest, with hundreds of

hours in both of the required spatial configurations in each region. Table 2 summarizes of the number of hours accumulated during the nominal 12-month Science Phase and Figs. 1 and 5 illustrate the residence time in the regions. Any time within the estimated bow shock is counted as within the magnetosphere (blue lines in Figs. 1 and 5), the connected fore-shock is defined based on if a typical Parker spiral magnetic field connects a point to the bow shock (green), while the remaining points are classified as pristine solar wind (red). Measurements from all instruments are recorded throughout the orbits outside of thruster operations, eclipses, and calibration activities and transmitted regardless of the Observatory configuration.

4.7 Mission Duration

As discussed in Sect. 3.1.2, SW parameters drive the behavior of turbulence, and more extreme values of these parameters are useful for distinguishing competing theories. To establish the minimum number of hours needed for HS science data sufficiency, we note that ~ 10 hours in extremely high (≥ 10) and low (≤ 0.1) plasma β enabled strong characterization of the spectral break, differentiating between predicted dissipation mechanisms (Chen et al. 2014). Using this assessment, the required number of hours of observation for the Baseline Mission was developed by analyzing two decades of Wind (Wilson et al. 2018; Klein and Vech 2019) data to ensure that we would adequately sample the full range of SW variability. Our methodology was to generate PDFs of parameters controlling turbulent behavior, e.g. SW speed (v_{SW}), plasma beta (β), proton temperature (T_p), balance of power between Sunward and anti-Sunward propagating fluctuations (cross helicity, σ_C (Parashar et al. 2018)), difference between kinetic and magnetic energy (residual energy σ_R (Wicks et al. 2013)), SW collisionality (Coulomb number N_C (Neugebauer 1976; Kasper et al. 2017)), and Alfvén Mach number (v_{SW}/v_A). Obtaining ~ 10 hours of measuring turbulence at relatively large and small values of these parameters determines the overall requirements for the number of hours in polyhedral and 3-D configurations; from the widths of the parameter PDFs, we determined that measuring 500 (100) hours in the 3D (polyhedral) configuration in the pristine SW, which then result in HS measuring 10 (2) hours of turbulence with extreme parameters both higher than the 98th percentile and lower than 2nd percentile of those values (corresponding to $\beta \sim 0.1$ and $\beta \sim 10$ (Chen et al. 2014)), a sufficient number of intervals at the very most extreme parameters to accomplish Mission science. Magnetosheath plasmas that will also be measured by HS typically have even higher values of $\beta_{\parallel,p}$ (Maruca et al. 2018). Measurements of these extreme intervals allow for the identification of different turbulent processes that are preferred in different parameter regimes, and will also be useful for providing accessible analogies to astrophysical systems where the thermal pressure dominates, e.g., the ISM ($\beta_{\parallel,p} \gtrsim 10$) or accretion disks ($\beta_{\parallel,p} \gtrsim 1$).

Large scale structures (LSS) generated by the Sun – e.g., CMEs, or produced as the SW propagates, e.g., CIRs can drive different kinds of turbulence compared to SW w/o LSS. By using *in situ* SW measurements of these structures over the last two solar cycles (Jian et al. 2018, 2019), we calculate the filling fraction during the 12-month Science Phase of these two kinds of structures for a 2028 Launch Readiness Date (LRD) based upon equivalent phases from Solar Cycles 23 and 24; the total anticipated LSS hours for this LRD are tabulated in Table 2.

The average CME filling fraction is 2.15% (1.9%/2.4% in Solar Cycle 23/24) while the CIR filling fraction is 16.8% (19.8%/13.8% in Solar Cycle 23/24). These rates correspond to 62 hours of CME observations, with 16/23 hours in 3D/polyhedral configurations and 484 hours of CIR measurements, with 131/179 hours in 3D/polyhedral configurations. We have

repeated this exercise for other LRDs, and found that regardless of launch date, there will be a sufficient number of hours of observed CMEs and CIRs to provide data to bring closure to G2O1.

4.8 Resilience, Redundancy, and Robustness of Multi-Satellite Observatory

Multi-SC swarm design offers innovations in flexibility and reconfiguration of the observatory. Orbital mechanics forces create continuously evolving relative positions among the 9 SC in HS. With known exceptions, the nominal swarm configuration has redundancy in most of the 3D baselines and tetrahedral vertices and accrues successful hours of science data collection well above the requirements.

Robustness above required performance and redundancy in spatial configurations create resilience in the event of contingencies. For the case of the loss of any one (or two) Nodes, the required number of hours in both configurations can be achieved within the duration of the 12-month Science Phase through a repositioning of the remaining Nodes to construct the configurations for which sufficient hours have not been achieved. A detailed discussion of Swarm Resiliency can be found in Joyner and Plice (2023).

4.9 Place Within the Heliospheric System Observatory

HS stands alone, but would also be part of the Heliospheric System Observatory (HSO) which provides additional opportunities for joint mission studies. Parker Solar Probe (PSP) (Fox et al. 2015) and Solar Orbiter (SoIO) (Müller et al. 2013) are making high-cadence plasma and IMF measurements of the innermost heliosphere. These inner-heliospheric missions provide only single point measurements, but these inform limits on injection scale structures that cascade into smaller structures as they propagate to 1 AU. Together with HS, and supplemented by Polarimeter to UNify the Corona and Heliosphere (PUNCH) imaging (DeForest et al. 2022), these observations allow for estimates of 1-AU-scale evolution and radial and longitudinal gradients. At intermediate scales (10^6 km), HS observations in combination with other missions in the HSO positions near the Sun-Earth L1 point (e.g., Advanced Composition Explorer (ACE) (Stone et al. 1998), Wind (Wilson et al. 2021), Interstellar Mapping and Acceleration Probe (IMAP) (McComas et al. 2018), Deep Space Climate Observatory (DSCOVR) (Loto'aniu et al. 2022)) provide opportunity for long-baseline correlations and to address the long-open question of local geometries of interplanetary shocks and flux ropes. These same HSO missions provide additional SW composition information to augment HS alpha particle measurements. Conjunctions with MMS (Burch et al. 2016) may also prove useful in extending the range of scales over which energy transfer and dissipation can be studied. Finally, given that energetic particle propagation is impacted by SW turbulence, ACE, Wind, Solar Terrestrial Relations Observatory (STEREO), and IMAP energetic particle measurements can test the effect of turbulence models and mechanisms HS quantifies. Joint study opportunities will depend on what HSO assets are operating when HS launches, but the breadth of the positions and instrumentation of missions within the HSO will enable a variety of examinations of fundamental processes at play in our Heliosphere.

5 HelioSwarm Mission Implementation

HS was selected as a Heliophysics Division Medium Explorer (MIDEX) mission by NASA Science Mission Directorate in 2022, and is currently in the formulation phase. MIDEX

missions are affordable testbeds for flagship science, from a cost and risk implementation perspective. The HS hardware and operations approach are all extremely high heritage to minimize overall project risk.

The HS architecture consists of one central Hub, an ESPA-class (EELV Secondary Payload Adapter) spacecraft provided by Northrop Grumman, and eight co-orbiting Nodes, SmallSats provided by Blue Canyon Technologies, both high heritage, 3-axis stabilized spacecraft. The Hub, Sect. 5.4, carries the eight Nodes to the science orbit. Pairs of Nodes will then separate from the Hub over four consecutive 14-day orbits. Each Node, Sect. 5.5, possesses identical instrument suites (IS) consisting of three high-heritage, high-TRL sensors optimized for HS: the Faraday Cup (FC, Sect. 5.2.1), provides high cadence measurements of the SW density and flow, and the Fluxgate Magnetometer (MAG, Sect. 5.1.1) and Search Coil Magnetometer (SCM, Sect. 5.1.2) provide measurements of the IMF at cadences sufficient to probe fluctuations from MHD to sub-ion scales. The Hub has the same IS as the Nodes, plus an ion Electrostatic Analyzer (iESA, Sect. 5.2.2), another high-heritage, high-TRL instrument that will provide high cadence measurements of the proton and alpha particles in order to characterize the local turbulence and to quantify ion heating. An electron Electrostatic Analyzer, (Sect. 5.3), included as a Student Collaboration Option for installation on the Hub, provides additional context for the plasma environment sampled by the HS Observatory.

The instruments were specifically selected to be both capable of addressing the science objectives when used as an Observatory and for having high heritage to ensure the fabrication, integration, and testing approaches for the required nine copies of flight model instruments, along with their costs and schedules, would be low risk.

5.1 Magnetometers

HS uses a combination of flux gate (MAG) and search coil (SCM) magnetometers to measure the IMF over the required frequency range indicated by Fig. 2 (DC \sim 3600 s to sub-ion $<$ 0.15 s). Two different magnetometer types are required owing to sensitivities required, especially at high frequencies (15 pT/Hz at 1 Hz and 1.5 pT/Hz at 10 Hz – see noise floors on Fig. 2); these same sensitivities impose mission requirements for DC and AC magnetic cleanliness. The MAG and SCM instruments overlap in frequency allowing for cross-calibration and the production of a merged data product, as has been performed for other missions (Fischer et al. 2016; Bowen et al. 2020).

5.1.1 Flux Gate Magnetometers (MAG)

The MAG is a dual core fluxgate magnetometer designed and built by Imperial College London (Imperial) which will be carried on every HS SC to measure the local magnetic field. The MAG design is based on direct heritage from the successful Solar Orbiter (Horbury et al. 2020) magnetometer (Fig. 7) with modifications taken from the recently launched JUICE (Jupiter ICy moons Explorer) instrument. HelioSwarm MAG will carry just one sensor on each spacecraft, at the end of a dedicated 3 m boom to minimise the effects of spacecraft fields, connected to the instrument electronics box via a harness. The electronics box will contain a power supply and Front End Electronics board: the latter will drive the sensor and digitise the signal, sending it directly to the spacecraft digital processing unit (DPU) where it will be filtered and decimated to 16 vectors/s on a common timeline with the SCM.

MAG data will be calibrated at Imperial College, with inter-calibration between S/C performed to ensure that derived products such as volumetric currents are reliably estimated.

Fig. 7 MAG is based on the flight-proven Solar Orbiter magnetometer design

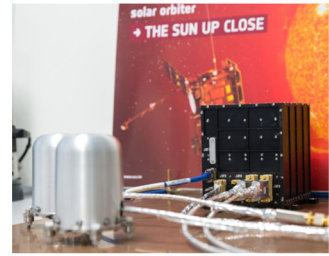


Table 3 Plasma and magnetic field observables measured across the HS Observatory. Required cadences, ranges, and accuracy for the measurements, as well as the projected performance and the instrument that will provide the measurement are organized by column

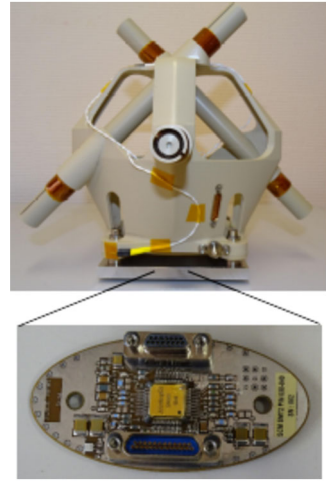
Observable	Requirement	Projected Performance	Instrument
Multi-point vector DC IMF \mathbf{B}	DC to 2-Sps ± 100 nT 0.15 nT per axis	DC to 16-Sps ± 128 nT 0.1 nT per axis	MAG (all SC)
Multi-point vector AC IMF \mathbf{B}	0.1 to 32-Sps $15/1.5$ pT/ $\sqrt{\text{Hz}}$ at 1/10 Hz	up to 32-Sps $6/0.6$ pT/ $\sqrt{\text{Hz}}$ at 1/10 Hz	SCM (all SC)
Multi-point proton density n_p	0.15 s $0.2\text{-}20$ cm $^{-3}$ $\pm 6\%$	0.125 s $0.1\text{-}50$ cm $^{-3}$ $\pm 5\%$	FC (all SC)
Multi-point proton velocity \mathbf{v}_p	0.15 s $250\text{-}800$ km/s $\pm 3\%$	0.125 s $212\text{-}840$ km/s Accuracy $\pm 1\%$	FC (all SC)
Single-point proton temperature T_p	0.3 s $10^4\text{-}5 \times 10^5$ K $\pm 5\%$	0.15 s $10^4\text{-}10^6$ K $\pm 1.8\%$	iESA (Hub)
Single-point temperature anisotropy $\frac{T_{\perp}}{T_{\parallel}}$	0.3 s 0.2-5 $\pm 6\%$	0.15 s 0.1-10 $\pm 3.4\%$	iESA (Hub)
Single-point α -proton density ratio $\frac{n_{\alpha}}{n_p}$	Hourly Averages 0-40% $\pm 10\%$	10 s 0-100% $\pm 3.4\%$	iESA (Hub)

MAG therefore contributes directly to the multi-point vector magnetic field measurement observable in Table 3, but is also central to the AC magnetic field measurement as well as some plasma products such as temperature anisotropies.

5.1.2 Search Coil Magnetometers (SCM)

The SCM is a heritage set of magnetic sensors designed and built by Laboratoire de Physique des Plasmas (LPP) and Laboratoire de Physique et Chimie de l'Environnement et de l'Es-

Fig. 8 JUICE SCM heritage instrument with its ASIC preamplifier



pace (LPC2E) selected to measure the IMF's higher frequencies needed to capture advected ion-scale structures. The HS SCM design is based on the most recent sensor developed for the ESA JUICE mission by LPP (Bergman and Wahlund 2022; Retinò 2020, 2023) (Fig. 8). LPP and LPC2E will be responsible for the testing and calibration of the instruments.

The SCM consists of a tri-axial set of 20 cm long magnetic sensors with associated preamplifier (ASIC) mounted at the tip of a 3 m boom opposite to the MAG boom. Each sensor axis consists of two windings (a primary and a secondary) around an internal PEEK mandrel inside which the ferromagnetic core (μ -metal) used on other flight heritage missions, (e.g. Cluster (Cornilleau-Wehrin et al. 2003) or THEMIS (Roux et al. 2008)) resides. Windings are connected to the preamplifier which drives the analog signal down the SCM boom harness to the IDPU which performs the digitization. SCM ground calibration is performed at the National Magnetic Observatory of Chambon-la-forêt using a facility upgraded by LPP for MMS and BepiColombo.

Each primary winding response is modified through a flux-feedback applied via a secondary winding to produce the frequency response and phase stability needed for Observatory-level analyses.

SCM has a single science operational mode drawing a steady 0.3 W. The three differential analog outputs of the SCM preamplifier are anti-alias filtered and digitized by the IDPU receiving electronics at 128 Sps then filtered to 32 Sps to satisfy HS observational requirements described in Table 3. This science operational mode is only interrupted during the in-flight calibration sequence. This sequence, scheduled for one per orbit and following events such as maneuvers and eclipses, will follow procedures successfully implemented on MMS, PSP, and Solo. It is performed to assess the stability of the transfer function through the mission using a calibration signal provided by the IDPU.

5.1.3 Magnetometer Operational Regions

The MAG and SCM instruments combined together cover the wide range of field magnitudes expected to be encountered in solar wind, magnetosphere, and foreshock regions. MAG operations are straightforward, with the instrument operating throughout the science orbit. The instrument will have a 4 pT resolution in its most sensitive range of ± 128 nT but

can range automatically up to 60,000 nT and can therefore operate in a full Earth field before launch. The sensitivity requirements on the measurement of the AC fluctuations are set to ensure that the relatively lower amplitude solar wind signals (e.g. Klein and Vech 2019; Pitřia et al. 2021) at ion-scale frequencies are resolved.

5.2 Ion Particle Detectors

In order to measure both the proton density and flow fluctuations as well as the proton temperatures, HS uses an ensemble of Faraday Cups mounted on each S/C as well as an ion Electrostatic Analyzer mounted only on the Hub. The co-location and overlapping field of views of the ion instruments on the Hub will allow for their cross-calibration.

5.2.1 Faraday Cups (FC)

The Faraday Cup (FC) is a heritage-based design developed at the Smithsonian Astrophysical Observatory (SAO), in conjunction with University of California, Berkeley (UCB), and Draper Laboratories. The sensor makes measurements of the radial VDFs of SW ions along with the flow angle of the incoming beam to measure proton densities and velocities over the ranges and sensitivities typical of the pristine SW.

Previous Faraday Cups have been employed on a wide variety of missions including Voyager (Bridge et al. 1977), Wind (Ogilvie et al. 1995), DSCOVR (Loto'aniu et al. 2022), and PSP (Case et al. 2020; Kasper et al. 2015). Two of the HS FC electronics boards (the logic/signal analysis board and the low-voltage power supply) are direct copies of the PSP electronics. A third board (the high-voltage power supply) is a fully-qualified backup design from the PSP instrument development. The instrument uses an oscillating electric potential to create an electric field that accepts or rejects particles based on their energy/charge. Particles with large enough E/q to successfully transit the electric field deposit their charge onto collector plates that measure the incoming current of SW particles.

A Faraday Cup instrument is placed on the sun-facing side of each spacecraft so that an unimpeded view is maintained in the direction of the Sun. Because Elsasser analysis involves measurements from both the IMF and SW, cross-sensor timing, pointing, and alignment requirements between the magnetometers and FC are levied.

The Faraday Cup operates in a single operational configuration throughout all phases of the mission. The instrument starts at its lowest voltage (energy/charge) and steps its way upward through 16 voltage windows while making measurements of the incoming SW current on each of its four collector plates in each window. The instrument keeps track of the maximum current measured in the previous spectrum so that the following spectrum can be measured with a more focused voltage range with better resolution.

The FC instrument design parameters have been determined by analyzing the historic distribution of all measurements made by the *Wind* Faraday Cup instrument. The aperture sizes, voltage ranges, and field-of-view for the HelioSwarm instrument are designed to capture more than 98% of the SW conditions (velocities, densities, and temperatures) that have been previously observed. The resulting voltage range will allow for measurement of proton velocities in the range of about 200-850 km/s. The FC mechanical design is shown in Fig. 9.

The Faraday Cup instruments provide a measurement of the radial distribution functions of the SW plasma on each of the nine spacecraft along with plasma quantities derived from those distributions. By calculating the moments of the distribution and by fitting an assumed functional form to the distribution, the vector velocity, density, and radial temperature can be provided. These data products contain 8 measurements per second and fulfill the multi-point measurement requirements of the velocity and density of the SW, as shown in Table 3.

Fig. 9 The Faraday Cup mechanical design (as of the concept study report). The mounting bracket is displayed in a semi-transparent mode. The instrument consists of two main subassemblies: the sensor (the top cylindrical section) and the electronics module (the lower rectangular box), which are connected by flexible coaxial cables

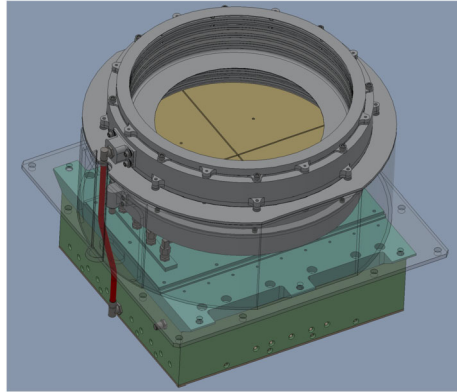
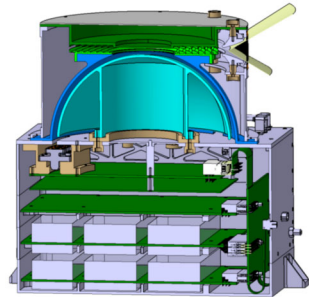


Fig. 10 iESA subsystem components (as of the concept study report), include the deflectors, collimators, and analyzer spheres (top), as well as the 16 channel electron multipliers, front end electronics, low- and high-voltage power supply, and FPGA board



5.2.2 Ion Electrostatic Analyzer (iESA)

The iESA is a particle sensor designed and built by Institut de Recherche en Astrophysique et Planetologie (IRAP, Toulouse, France), Laboratoire d'Astrophysique de Bordeaux (LAB, Pessac, France), University of New Hampshire (UNH, USA), and Mullard Space Science Laboratory (MSSL, UK), with IRAP technical leadership and heritage. The direct heritage instrument is the Proton and Alpha Sensor (Owen et al. 2020) onboard the Solar Orbiter mission (Müller et al. 2020), with some sub-systems inherited from other past particle instrumentation led by IRAP (on STEREO, MAVEN, Cluster, etc.). iESA measures the full proton and alpha particle distribution functions with an unprecedented combination of high energy, angular and time resolutions (cf. Table 3).

As illustrated in Fig. 10, entrance deflectors allow for the sweeping of input elevation angles $\pm 24^\circ$ from the main detection plane with 3° angular binning, which is resolvable with the use of a collimator. The deflected and collimated ions are then subject to E/q selection through a classic top-hat electro-static analyzer. The E/q selected ions are focused onto the main detection plane, which comprises 16 channel electron multipliers (CEMs). These perform a 10^7 gain in charge collection on anodes with 3° resolution in azimuth over an angular range of $\pm 24^\circ$ as well, allowing for a homogeneous $\pm 24^\circ$ field-of view with 3° angular resolutions, in both elevation and azimuth angles. The iESA electronics contains (1) a front-end board comprising 16 CEMs with associated anodes and amplifiers, (2) a high-voltage board to supply the entrance deflectors, analyzer plates, and CEMs with the required (static or sweeping) high voltages, as well as (3) an FPGA and (4) a low-voltage power supply board dedicated to instrument control and power.

iESA operations are based on the sequential stepping of the electrostatic analyzer and entrance deflector high voltages. The instrument implements SW beam-tracking strategies (Owen et al. 2020), using previous measurements, to dynamically set the energy and angular bins of the next sample, allowing for faster measurement cadence. The iESA is highly versatile and the tracking strategy can implement any combination of energies and angles. Instrument operation will be adapted to the science target, but a primary operation mode is expected to be a Proton Tracking mode measuring the 3D VDFs of SW protons with high energy (8%) and angular (3°) resolutions at a cadence down to 150 ms, well into the sub-ion timescales. To characterize alphas, a Proton-Alpha Tracking mode will be used, with 48 energy bins and a 450 ms cadence, though longer accumulation times can be used to enhance counting statistics as needed.

5.2.3 Ion Detector Operational Regions

To demonstrate the regions from the HS orbits that the ion instruments will resolve the proton distribution, we employ ion density and velocity moment data from the THEMIS-ARTEMIS mission in lunar orbit (Angelopoulos 2011) aggregated from all measurements made by the electrostatic analyzer (McFadden et al. 2008) on probe P1 outside of the lunar wake during the calendar year 2017, approximately one solar cycle before the HS nominal mission; see Fig. 11. As THEMIS-ARTEMIS's lunar orbit is at a similar distance as HS's apogee, where much of the observatory's science data will be collected, we take these observations to be representative of the plasma HS will encounter.

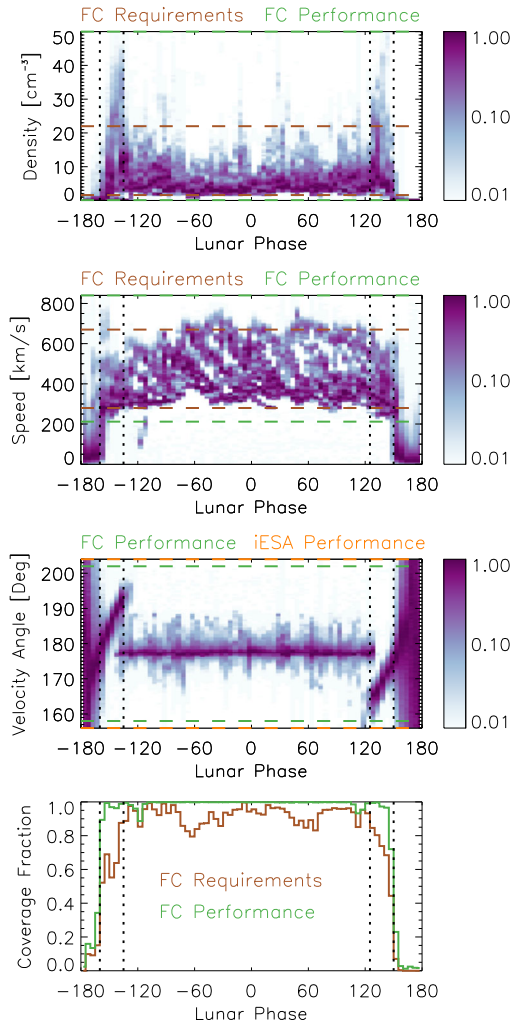
The top three panels show normalized frequency distributions of observed quantities as a function of lunar phase, defined such that the new moon occurs at a phase of 0 (in the solar wind) and the full moon occurs at a phase of 180 (in the terrestrial magnetosphere). Each 2D frequency distribution is normalized so that the most frequently observed value of the quantity at each lunar phase has a relative frequency of 1.0; the color of each bin thus represents the relative frequency of observation of that value of the quantity at that lunar phase.

Brown horizontal dashed lines show level one FC requirements, green horizontal dashed lines show expected FC performance, and orange horizontal dashed lines show expected iESA performance. The brown histogram in the bottom panel shows the fraction of observations at each lunar phase for which the observed density and flow speed lie within the level one FC requirement ranges and the velocity angle lies in the FC field of view, while the green histogram shows the fraction of observations within the expected FC performance ranges. Vertical dotted black lines in all panels mark the approximate location of the outbound and inbound magnetopause and bow shock crossings. We see that in the solar wind, between $\approx \pm 120^\circ$, the FCs are expected to resolve the proton distribution nearly all of the time. This continues to hold between the magnetopause and bow shock, with the FCs losing the ability to resolve the protons further inside the magnetosphere due to a significant drop in the proton speed.

5.3 Student Electron Electrostatic Spectrograph Student Collaboration

In addition to the magnetic field and ion instruments previously listed in this section, HS has also proposed to include a Student Electron Electrostatic Spectrograph (SEE) Student Collaboration project to measure ambient, low energy electrons. This electron instrument would be mounted on the Hub SC, and would be used to study the connectivity of the local magnetosphere, solar wind, and cis-lunar space via measurements of low-energy electron

Fig. 11 Normalized distributions of ion density (top panel), speed (second) and velocity angle (third) measured by THEMIS-ARTEMIS as a function of lunar phase, described in detail in Sect. 5.2.3, compared to FC requirements (brown) and expected FC (green) and iESA (orange) performance. The bow shock and magnetopause crossings are illustrated with vertical dashed lines. The bottom panel illustrates the fraction of the time that ions will be resolved for both the FC requirements and expected performance

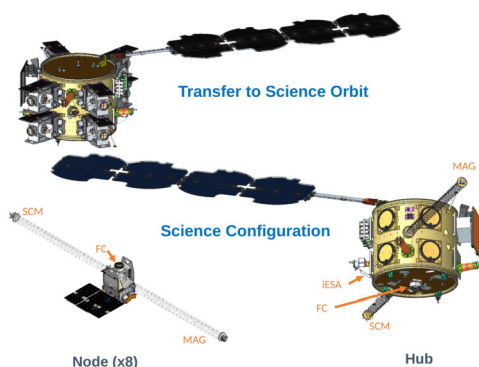


populations. The project would be co-led by graduate and undergraduate students, with the prime deliverable from the SEE project a cohort of future scientists educated in the lifecycle of a NASA mission, including instrument development and merger of science goals with hardware design. The SEE measurements will be independently valuable, and potentially augment the measurements made by the overall HS observatory by adding additional context regarding the behavior of electrons in a variety of turbulent environments. A backup design for SEE has PSP and ESCAPE flight heritage (Whittlesey et al. 2020).

5.4 The Hub

Northrop Grumman (NG) provides the Hub spacecraft. This ESPA-class spacecraft serves as the central relay for all Nodes within the Observatory and is based on the high-heritage ESPStar line which was designed to carry separable payloads to orbit. The Hub is 730 kg at launch, including the hydrazine propellant necessary for carrying it and all the Nodes

Fig. 12 Transfer (top) and Science (bottom) Configurations for the Hub (Sect. 5.4) and Node (Sect. 5.5) S/C



into the HS science orbit, illustrated at the top of Fig. 12. The Hub is capable of generating 1165 W of power via its single deployable solar array. As configured for science, the Hub spans a maximum dimension of 8.4 m.

5.5 The Nodes

The Node spacecraft are Blue Canyon Technologies (BCT) Venus-class spacecraft with standard accommodations for hosting the HS payload. As configured for HS, the SmallSat Nodes are just over 70 kg each and use onboard propulsion to maintain the proper swarm geometry. The Nodes generate 200 W of power and provide a single mechanical interface to the HS payload. With booms deployed, bottom left of Fig. 12, the maximum tip-to-tip dimension of the Nodes is just over 6 m.

5.6 Observatory Architecture

The HS flight system will launch with the Hub carrying all 8 Nodes through a series of phasing loops and a lunar swingby into the science orbit over a period of approximately 72 days. Once the science orbit (a High Earth Orbit P/2 lunar resonant orbit with apogee greater than $60R_E$ and perigee less than $12R_E$), pairs of Nodes are separated from the Hub spacecraft and instrument checkouts and calibrations occur during the ≈ 81 -day commissioning phase. Once the Nodes have been maneuvered into their proper locations in the observatory, the 12-month science phase begins. HS uses a hub-and-spoke communications architecture in which the Hub is the only direct link to the ground (via S-band, DSN) and each Node receives commands from and relays science data directly to the Hub via S-band crosslinks.

The Mission Operations Center (MOC) is hosted out of ARC, with engineering support centers for Hub and Nodes at NG and BCT respectively. The Science Operations Center (SOC) is hosted out of the PI-institution, UNH, which is also responsible for delivering L1-L4 data products to NASA SPDF; see Sect. 5.7. The HS missions operations approach strategically uses the inherent orbital dynamics of the observatory; the swarm naturally “expands” and “contracts” over each 14-day orbital period. The Flight Dynamics team has designed the staggering of the Node-Hub closest approaches around perigee to facilitate periods of high-rate data downlink for each Node each orbit. As the observatory begins to expand out towards apogee, the polyhedral performance, Sect. 4.5.2, requirements are satisfied. At apogee and on the contraction back in towards perigee, the longest-baseline 3D performance requirements are satisfied, Sect. 4.5.1.

5.7 Data Processing and Selection

The Science Data Center (SDC) at the UNH SOC supports HS data processing, produces timing and other ancillary data that are provided to the instrument teams, releases and archives L0-L4 data with associated calibrations, and provides data selection tools to the community.

Automated processes transfer L0 telemetry data from the HS MOC to the SOC within 24 hours of ground receipt. Upon L0 receipt, the SOC performs packet format checks (e.g., valid headers, checksums). The SOC prepares a timing product to correct Node clock differences relative to the Hub timing and processes IS housekeeping (HK) to calibrated units (L1). L0 data are provided to the instrument teams for processing, with timing corrections and L1 HK included as additional inputs. The instrument teams generate and validate L1 (measurements in engineering units), L2 (science data—magnetic field measurements, particle velocity distributions and the associated moments and fits—in payload coordinates), and L3 (science data in RTN coordinates) data products within 30 days of receipt.

L1-L3 data are retrieved by the SOC from the instrument teams within 24 hours of processing and summary plots generated. L4 data products, e.g. a merger of the MAG and SCM data or combined magnetic field and proton products from across the observatory, are produced at the SOC within 5 working days.

Upon completion of IS commissioning, the SOC begins a period of data product and instrument performance validation. As data for each orbit are downlinked, they are routinely and automatically processed. During the subsequent orbit, the SDC lead coordinates instrument team validation of the data. Validation activities proceed through individual calibration and Observatory-level calibrations. As calibrations are updated, previous orbits' data are re-processed with the updated calibrations, so the process iterates with increasing data volumes of increasing refinement. Validated, calibrated L2 through L4 data are provided to NASA SPDF for public access upon completion of the validation period, anticipated to be no more than 5 months, which may be shortened if reasonable calibrations are available sooner.

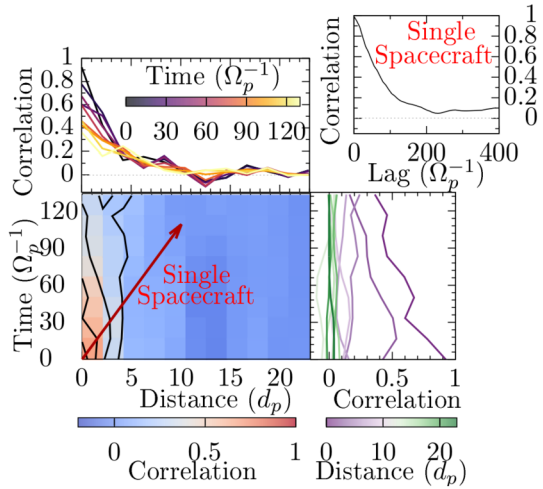
Because HS comprises nine spacecraft with slowly changing relative positions in an equally dynamic plasma environment, specialized tools to assist researchers in their data selection will be developed and implemented at the SOC. Many techniques employed by the researchers require specific Observatory configurations. To aid the researcher in the selection of processed data, the SOC is developing interactive queries, but all science data are downlinked and processed regardless of observatory configuration. As an example, Fig. 5 shows a snapshot from a preliminary data selection code using DRM orbit trajectories.

6 Analysis Approaches

A variety of multi-spacecraft Analysis Approaches have been previously developed for missions such as Cluster and MMS. These methods include calculations of

- **Cascade Rate**, measuring of the transfer of turbulent fluctuation energy from one spatial scale to another (e.g. Hadid et al. 2018; Pecora et al. 2023),
- **2-point correlation**, measuring the temporal and spatial scale over which a spectral element is remade by nonlinear processes (e.g. Horbury 2000; Matthaeus et al. 2016),
- **Structure Functions**, determining the statistics turbulent field increments to reveal scale-dependent, intermittent turbulence (e.g. Sreenivasan and Antonia 1997; Chhiber et al. 2021),

Fig. 13 The spatial-temporal correlation calculated from synthetic HS measurements extracted from a hybrid-PIC simulation of turbulence (Arzamasskiy et al. 2019). By using all nine trajectories, we are able to resolve the spatial and temporal dependences of Eqn. (4) independently, unlike the auto-correlation from a single trajectory, presented in the upper right-hand panel, which effectively samples along the red arrow in the lower left panel, convolving together spatial and temporal variations



- **Wave telescope**, determining the wavevectors of plasma waves and their associated 3D power distributions (e.g. Pincon and Lefeuvre 1991; Narita et al. 2022),
- **Pressure-strain interaction**, measuring the dilation, $-(\underline{P} \cdot \nabla) \cdot \underline{U}$, which describes the local conversion between flow and thermal energy (e.g. Yang et al. 2017; Cassak and Barbhuiya 2022; Roberts et al. 2023),
- **Curlometer & Gradient Methods**, which construct current sheets and other intermittent structures from spatially distributed measurements (e.g. Dunlop et al. 2002b, 2021).

Many of these methods and their applications have been documented in ISSI review articles over the last several decades (Paschmann and Daly 1998, 2008). In this section, we apply some analysis approaches to synthetic timeseries constructed using DRM trajectories corresponding to selected HS configurations through different numerical simulations of turbulence including two-fluid (Wang et al. 2015; Juno et al. 2018) and hybrid-PIC (Kunz et al. 2014; Arzamasskiy et al. 2019) nonlinear simulations and quasilinear simulations (Klein et al. 2012, 2014). We note that due to computational limitations, all the numerical codes used make approximations in terms of the physical processes included and/or the scales simulated. Therefore, we do not expect the numerical simulations to be completely representative of actual plasma turbulence at all scales, and differences between simulations and HS observations will drive improvements of the modeling of turbulent transport and dissipation.

6.1 Multipoint Correlations and Structure Functions

Multipoint spectral analysis, 2nd-order structure functions, and space-time correlation functions yield distributions of turbulent energy in configuration space (Chen et al. 2011; Paschmann and Daly 1998, 2008) and, through time-lagging, decorrelation times for fluctuations at measured spatial scales (Matthaeus et al. 2016).

Figure 13 illustrates the temporal and spatial decorrelation of signals from synthetic magnetic field data set constructed by sampling a hybrid-PIC numerical simulation (Arzamasskiy et al. 2019) over trajectories defined by the DRM described in Sect. 4.6. The correlation is calculated between all nine trajectories at each point in the timeseries as

$$R(|\mathbf{r}|, \tau) = \langle \mathbf{b}(\mathbf{x}, t) \cdot \mathbf{b}(\mathbf{x} + \mathbf{r}, t + \tau) \rangle. \tag{4}$$

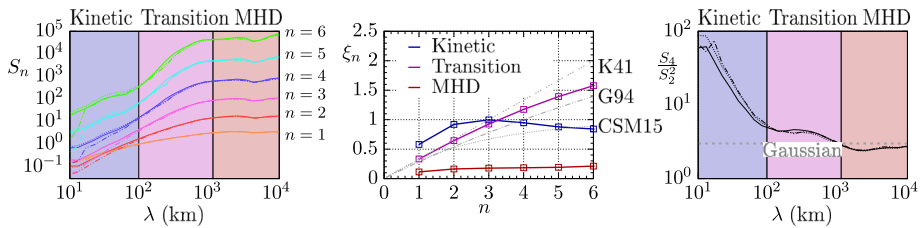


Fig. 14 HS’s multiscale configuration enables the calculation of multiple orders of structure functions (left panel), that when fit to a power-law $S_n \propto \lambda^{\xi_n}$ (center) or recombined into quantities such as kurtosis S_4/S_2^2 (right) can be compared to theoretical predictions (e.g. Kolmogorov 1941; Grauer et al. 1994; Chandran et al. 2015) to characterize the scale-dependent intermittency in turbulence (G1O4)

These correlation values, and how quickly they depart from unity, characterizes the temporal and spatial scales over which fluctuations are remade by nonlinear terms, and represents a key statistical property of turbulent distributions (Matthaeus et al. 2005) that will be used in G1O1 and G1O2. For comparison, an example auto-correlation produced using lagged timeseries from a single trajectory (upper right panel) mixes together spatial and temporal dependence. HS will disentangle spatial and temporal correlations which single SC convolve together.

The measurement of intense fluctuations at smaller scales while simultaneously measuring the distribution of fluctuations at larger scales differentiates between models of scale-dependent intermittency, testing theoretical predictions (Tennekes 1975; Grauer et al. 1994; Chandran et al. 2015; Mallet and Schekochihin 2017; Greco et al. 2009). Intermittency also affects different types of proton heating mechanisms in different ways, with the associated coherent structures greatly affecting the efficiency of certain processes. For example, stochastic heating occurs when fluctuation amplitudes at the scale of a particle’s gyroradius become large (Chandran et al. 2010; Dalena et al. 2014), which are enhanced near coherent structures. Conversely, dissipation mechanisms such as Landau damping are less affected by intermittency (Mallet et al. 2019). HS multiscale measurement of higher order intermittent statistical measures, along with temperature and temperature anisotropy reveal deep connections between cascade, intermittency and dissipation.

One means of quantifying the intermittency of a system is illustrated in Fig. 14, where we calculate the scale-dependent structure function S_n using synthetic times series drawn from the same hybrid numerical simulation of turbulence (Arzamasskiy et al. 2019). Instead of using increments drawn from a single timeseries

$$S_n(\lambda = \tau v_{SW}) = \langle [\delta z(t + \tau) - \delta z(t)]^n \rangle \tag{5}$$

(Chhiber et al. 2021), increments are calculated using all nine timeseries combined with HS’s spatial resolution and configurations and a modified form of Taylor’s hypothesis (Horbury 2000) allowing for orders of magnitude more samples to be used at a given scale both along and transverse to the magnetic field and flow directions,

$$S_n[\mathbf{x}_i(t + \tau) - \mathbf{x}_j(t)] = \langle \{ \delta z[\mathbf{x}_i(t + \tau)] - \delta z[\mathbf{x}_j(t)] \}^n \rangle \tag{6}$$

enabling the calculation of the higher order structure functions spanning ion kinetic (blue, left panel), transition (purple), and MHD (red) scales; for N increments measured, structure functions of order $n = \log_{10}[N] - 1$ can be resolved (Dudok de Wit 2004; Dudok de Wit

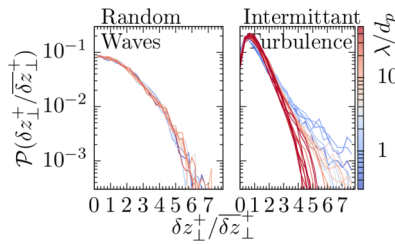


Fig. 15 HS measures intermittency at MHD (red) and sub-ion (blue) scales simultaneously from different numerical simulations, providing science closure on G1O4 by differentiating between models of nonlinear coupling that predict enhanced amplitudes of normalized Elsasser fluctuations δz_{\perp}^{\pm} at small scales (right, from a turbulent hybrid-PIC simulation (Arzamasskiy et al. 2019)) compared to a scale-independent normal distribution of amplitudes (left, drawn from ensemble of randomly-phased wave modes)

et al. 2013); HS enables the study of higher order S_n than previous missions, where differences between theoretical descriptions are more easily distinguishable. From these measurements of S_n , theories about intermittency as a function of scale (Sreenivasan and Antonia 1997), which describe how frequently and how abruptly sharp structures of different sizes and shapes arise, are tested by fitting $S_n \propto \lambda^{\xi_n}$ over different scale ranges (center); the trending of the fit parameters with order n is used to validate, falsify, or improve theories [e.g. Kolmogorov (1941), Grauer et al. (1994), Chandran et al. (2015)]. Combined with other metrics such as kurtosis (right panel) as well as the analysis method presented in Fig. 15, HS characterizes turbulent intermittency as a function of scale addressing G1O4.

Figure 15 illustrates with the same simulated synthetic DRM timeseries used for Fig. 13 another way in which HS will provide science closure on G1O4 by using its 36 baseline separations to simultaneously quantify the distribution of turbulent fluctuations at large and small scales. Following Mallet et al. (2015), we define the fluctuation amplitude increment

$$\delta z_{\perp}^{\pm} = |\delta \mathbf{z}_{\perp}^{\pm}| = |\mathbf{z}_{\perp}^{\pm}(\mathbf{r}_0 + \mathbf{r}_{\perp}) - \mathbf{z}_{\perp}^{\pm}(\mathbf{r}_0)| \tag{7}$$

where \mathbf{r}_{\perp} is the separation in the plane perpendicular to the mean magnetic field direction \mathbf{B}_0 . Using both the synthetic HS timeseries drawn from a hybrid-PIC simulation, as well as timeseries constructed from a collection of randomly phased waves, we calculate δz_{\perp}^{\pm} as a function of scale $\lambda = |\mathbf{r}_{\perp}|$ for an ensemble of separations. We then calculate the median value of the increment δz_{\perp}^{\pm} over a series of bins spaced logarithmically in λ , and normalize the probability distribution function of the increments in each bin by the median. For the trivial case of randomly-phased waves, the increments are normally distributed, and there is no variation as a function of scale. For the case of simulated turbulence, the intermittency increases with decreasing scale, seen in the transition from red (large, MHD scales) to blue (smaller, ion-kinetic scales). As the intermittency of a turbulent system depends on the nature of the nonlinear interactions that transport energy through a system, these types of distributions represent a sensitive test of different models of turbulence.

6.2 Curlometer and Gradient Techniques

Wave telescope and curlometer techniques reveal the nature of fluctuations and identify structures within turbulence. Gradient estimation is closely related and is required for determining the pressure-strain tensor and the production rate of internal energy.

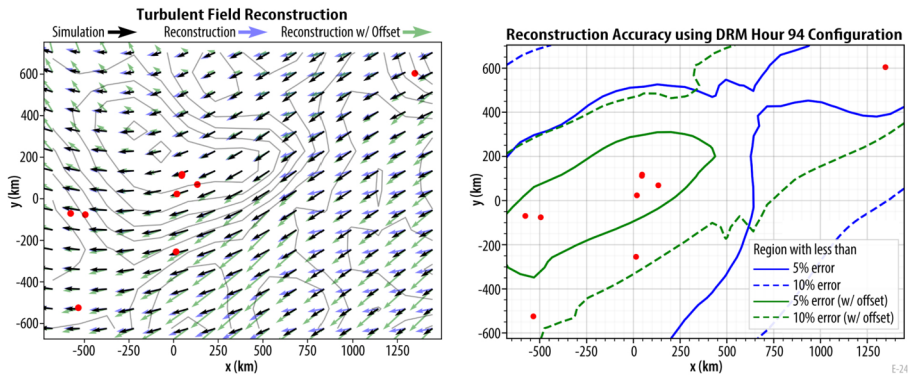


Fig. 16 HS's SC positions (red points) enable a high-fidelity reconstruction (perfect measurements shown in blue, measurements with included systematic errors in green) of the magnetic field (arrows) over a larger volume of space, enabling the simultaneous study of ion-scale structures (e.g., current sheets, shown as contours at left) with sufficient accuracy to address G1O4 (regions of reconstruction with less than 5% and 10% error shown at right, as explained in the text)

As an example of a novel application of gradient techniques enabled by a multi-spacecraft observatory, estimates for the spatial gradients from synthetic timeseries drawn from a two-fluid numerical simulation of turbulence (Wang et al. 2015) are used in a first-order reconstruction to reconstruct a 3D synthetic magnetic field, shown in Fig. 16 and described in detail in Broeren et al. (2021). By using a weighted average of the first-order estimates for the reconstructed magnetic field drawn from the spatial gradients determined from the 126 unique tetrahedra that comprise the HS Observatory, we accurately reproduce the magnetic field over large volumes of the simulation. For a selected DRM interval in a good polyhedral configuration, we reconstruct the simulated turbulent magnetic field (black/blue arrows indicate the simulated/reconstructed field). Averaging over many spatial locations in the simulation, this analysis method yields $\leq 5\%$ relative error over a volume of nearly $1.82 \times 10^9 \text{ km}^3$ (solid blue line, right panel) and $\leq 10\%$ error over a volume of $3.208 \times 10^9 \text{ km}^3$ (dashed blue line).

To quantify the impact of systematic errors on this analysis technique, we introduce random offsets replicating estimated systematic errors to each component of the measured magnetic field at all nine SC (green lines). This produces reconstructed volumes of $3.66 \times 10^8 (1.77 \times 10^9) \text{ km}^3$ for the 5% (10%) error thresholds. By leveraging the large number of tetrahedral configurations sensitive to many length scales simultaneously, HS enables simultaneous studies of both MHD-scale structure as well as much smaller current sheets, bringing closure to questions about the transfer of energy from fields to flows (G1O3) and associated heating near ion-scale intermittent structures (G1O4).

As discussed at the beginning of this section, several other multispacecraft analysis methods, previously implemented on missions such as MMS and Cluster, can be immediately applied to HS observations, or extended to incorporate information from all nine spacecraft in the observatory, as demonstrated in recent publications (Perri et al. 2017; Zhang et al. 2021; Pecora et al. 2023; Toepfer et al. 2023), including estimates for the errors associated with these multi-spacecraft methods (Broeren et al. 2021; Broeren and Klein 2023; Roberts et al. 2023).

7 Conclusions

Turbulence is the process by which energy contained in fluctuating magnetic fields and plasma motion cascades from larger to smaller spatial scales, and ultimately into thermal energy of charged particles comprising the plasma. In addition to being a key process that heats cosmic plasmas, it also creates the conditions in which all universal plasma processes (e.g., magnetic reconnection, shocks, particle acceleration) act, both within the heliosphere and in all astrophysical domains. Due to its fundamentally multiscale nature, only spatially distributed, simultaneous measurements provide the data needed to bring closure to outstanding questions about the distribution and transfer of turbulent energy. HS achieves its mission objectives through an innovative swarm implementation of high-heritage mission elements, ranging from instruments, to spacecraft, operations, and analysis tools. HS provides a paradigm shift in mission design where the many elements of the swarm and the way they interact form an Observatory that is far more than the sum of its parts. As the first multipoint, multiscale mission, HS gives an unprecedented view into the nature of space plasma turbulence.

Supplementary Information The online version contains supplementary material available at <https://doi.org/10.1007/s11214-023-01019-0>.

Acknowledgements We are deeply indebted to the incredible members of the HelioSwarm science, engineering, and proposal teams whose tireless efforts enabled this mission.

Funding Construction and analysis of the HelioSwarm Observatory Design Reference Mission trajectories was supported in part by the HelioSwarm Project funded under NASA's Prime contract no. 80ARC021C0001. Support was also provided by grant UKRI/STFC ST/W001071/1.

Declarations

Competing Interests The authors declare no competing interests.

Open Access This article is licensed under a Creative Commons Attribution 4.0 International License, which permits use, sharing, adaptation, distribution and reproduction in any medium or format, as long as you give appropriate credit to the original author(s) and the source, provide a link to the Creative Commons licence, and indicate if changes were made. The images or other third party material in this article are included in the article's Creative Commons licence, unless indicated otherwise in a credit line to the material. If material is not included in the article's Creative Commons licence and your intended use is not permitted by statutory regulation or exceeds the permitted use, you will need to obtain permission directly from the copyright holder. To view a copy of this licence, visit <http://creativecommons.org/licenses/by/4.0/>.

References

- Alexandrova O (2008) Solar wind vs magnetosheath turbulence and Alfvén vortices. *Nonlinear Process Geophys* 15(1):95–108. <https://doi.org/10.5194/npg-15-95-2008>
- Alexandrova O, Carbone V, Veltri P, Sorriso-Valvo L (2008) Small-scale energy cascade of the solar wind turbulence. *Astrophys J* 674:1153–1157. <https://doi.org/10.1086/524056>. [arXiv:0710.0763](https://arxiv.org/abs/0710.0763)
- Alexandrova O, Chen CHK, Sorriso-Valvo L, Horbury TS, Bale SD (2013) Solar wind turbulence and the role of ion instabilities. *Space Sci Rev* 178(2–4):101–139. <https://doi.org/10.1007/s11214-013-0004-8>
- Ambrosiano J, Matthaeus WH, Goldstein ML, Plante D (1988) Test particle acceleration in turbulent reconnecting magnetic fields. *J Geophys Res* 93(A12):14383–14400. <https://doi.org/10.1029/JA093iA12p14383>
- Angelopoulos V (2008) The THEMIS mission. *Space Sci Rev* 141(1):5. <https://doi.org/10.1007/s11214-008-9336-1>

- Angelopoulos V (2011) The ARTEMIS mission. *Space Sci Rev* 165(1–4):3–25. <https://doi.org/10.1007/s11214-010-9687-2>
- Armstrong JW, Cordes JM, Rickett BJ (1981) Density power spectrum in the local interstellar medium. *Nature* 291(5816):561–564. <https://doi.org/10.1038/291561a0>
- Arzamasskiy L, Kunz MW, Chandran BDG, Quataert E (2019) Hybrid-kinetic simulations of ion heating in Alfvénic turbulence. *Astrophys J* 879(1):53. <https://doi.org/10.3847/1538-4357/ab20cc>
- Balbus SA, Hawley JF (1998) Instability, turbulence, and enhanced transport in accretion disks. *Rev Mod Phys* 70(1):1–53. <https://doi.org/10.1103/RevModPhys.70.1>
- Bandyopadhyay R, Chasapis A, Chhiber R, Parashar TN, Maruca BA, Matthaeus WH, Schwartz SJ, Eriksson S, Le Contel O, Breuillard H (2018) Solar wind turbulence studies using MMS fast plasma investigation data. *Astrophys J* 866(2):81. <https://doi.org/10.3847/1538-4357/aade93>
- Bandyopadhyay R, Chasapis A, Chhiber R, Parashar TN, Matthaeus WH, Shay MA, Maruca BA, Burch JL, Moore TE, Pollock CJ, Giles BL, Paterson WR, Dorelli J, Gershman DJ, Torbert RB, Russell CT, Strangeway RJ (2018) Incompressible energy transfer in the Earth's magnetosheath: magnetospheric multiscale observations. *Astrophys J* 866(2):106. <https://doi.org/10.3847/1538-4357/aade04>
- Bandyopadhyay R, Goldstein ML, Maruca BA, Matthaeus WH, Parashar TN, Ruffolo D, Chhiber R, Usmanov A, Chasapis A, Qudsi R, Bale SD, Bonnell JW, Dudok de Wit T, Goetz K, Harvey PR, MacDowall RJ, Malaspina DM, Pulupa M, Kasper JC, Korreck KE, Case AW, Stevens M, Whittlesey P, Larson D, Livu R, Klein KG, Velli M, Raouafi N (2020) Enhanced energy transfer rate in solar wind turbulence observed near the sun from Parker Solar Probe. *Astrophys J Suppl* 246(2):48. <https://doi.org/10.3847/1538-4365/ab5dae>
- Bandyopadhyay R, Matthaeus WH, Chasapis A, Russell CT, Strangeway RJ, Torbert RB, Giles BL, Gershman DJ, Pollock CJ, Burch JL (2020a) Direct measurement of the solar-wind Taylor microscale using MMS turbulence campaign data. *Astrophys J* 899(1):63. <https://doi.org/10.3847/1538-4357/ab9ebe>
- Bandyopadhyay R, Matthaeus WH, Parashar TN, Yang Y, Chasapis A, Giles BL, Gershman DJ, Pollock CJ, Russell CT, Strangeway RJ, Torbert RB, Moore TE, Burch JL (2020b) Statistics of kinetic dissipation in the Earth's magnetosheath: MMS observations. *Phys Rev Lett* 124(25):255101. <https://doi.org/10.1103/PhysRevLett.124.255101>
- Belcher JW, Davis L Jr (1971) Large-amplitude Alfvén waves in the interplanetary medium, 2. *J Geophys Res* 76:3534. <https://doi.org/10.1029/JA076i016p03534>
- Bergman J, Wahlund JE (2022) The Radio and Plasma Wave Investigation (RPWI) for the Jupiter ICy moons Explorer (JUICE). In: *Europlanet Science Congress. EPSC Abstracts*, p 838. <https://doi.org/10.5194/epsc2022-838>
- Bieber JW, Wanner W, Matthaeus WH (1996) Dominant two-dimensional solar wind turbulence with implications for cosmic ray transport. *J Geophys Res* 101:2511–2522. <https://doi.org/10.1029/95JA02588>
- Boldyreva S (2006) Spectrum of magnetohydrodynamic turbulence. *Phys Rev Lett* 96(11):115002. <https://doi.org/10.1103/PhysRevLett.96.115002>
- Borovsky JE, Denton MH, Smith CW (2019) Some properties of the solar wind turbulence at 1 AU statistically examined in the different types of solar wind plasma. *J Geophys Res Space Phys* 124(4):2406–2424. <https://doi.org/10.1029/2019JA026580>
- Bowen TA, Bale SD, Bonnell JW, Dudok de Wit T, Goetz K, Goodrich K, Gruesbeck J, Harvey PR, Jannet G, Koval A, MacDowall RJ, Malaspina DM, Pulupa M, Revillet C, Sheppard D, Szabo A (2020) A merged search-coil and fluxgate magnetometer data product for Parker solar probe FIELDS. *J Geophys Res Space Phys* 125(5):27813. <https://doi.org/10.1029/2020JA027813>
- Breech B, Matthaeus WH, Minnie J, Bieber JW, Oughton S, Smith CW, Isenberg PA (2008) Turbulence transport throughout the heliosphere. *J Geophys Res Space Phys* 113(A8):08105. <https://doi.org/10.1029/2007JA012711>
- Bridge HS, Belcher JW, Butler RJ, Lazarus AJ, Mavretic AM, Sullivan JD, Siscoe GL, Vasyliunas VM (1977) The plasma experiment on the 1977 Voyager mission. *Space Sci Rev* 21(3):259–287. <https://doi.org/10.1007/BF00211542>
- Broeren T, Klein KG (2023) Data-driven uncertainty quantification of the wave telescope technique: general equations and demonstration using HelioSwarm. *Astrophys J Suppl* 266(1):12. <https://doi.org/10.3847/1538-4365/acc6c7>
- Broeren T, Klein KG, TenBarge JM, Dors I, Roberts OW, Verscharen D (2021) Magnetic field reconstruction for a realistic multi-point, multi-scale spacecraft observatory. *Front Astron Space Sci* 8:727076. <https://doi.org/10.3389/fspas.2021.727076>
- Brown MR, Schaffner DA (2015) SSX MHD plasma wind tunnel. *J Plasma Phys* 81(3):345810302. <https://doi.org/10.1017/S0022377815000227>
- Bruno R, Carbone V (2013) The solar wind as a turbulence laboratory. *Living Rev Sol Phys* 10(1):2. <https://doi.org/10.12942/lrsp-2013-2>

- Burch JL, Hwang K-J (2021) Exploring small scales with MMS. In: Maggiolo R, André N, Hasegawa H, Welling DT (eds) *Magnetospheres in the solar system*, vol 2, p 657. <https://doi.org/10.1002/9781119815624.ch41>
- Burch JL, Moore TE, Torbert RB, Giles BL (2016) Magnetospheric multiscale overview and science objectives. *Space Sci Rev* 199(1):5–21. <https://doi.org/10.1007/s11214-015-0164-9>
- Case AW, Kasper J, Stevens ML, Korreck KE, Paulson K, Daigneau P, Caldwell D, Freeman M, Henry T, Klingensmith B, Bookbinder JA, Robinson M, Berg P, Tiu C, Wright JKH, Reinhart MJ, Curtis D, Ludlam M, Larson D, Whittlesey P, Livi R, Klein KG, Martinović MM (2020) The solar probe cup on the Parker solar probe. *Astrophys J Suppl* 246(2):43. <https://doi.org/10.3847/1538-4365/ab5a7b>
- Cassak PA, Barbhuiya MH (2022) Pressure-strain interaction. I. On compression, deformation, and implications for Pi-D. *Phys Plasmas* 29(12):122306. <https://doi.org/10.1063/5.0125248>
- Chandran BDG, Li B, Rogers BN, Quataert E, Germaschewski K (2010) Perpendicular ion heating by low-frequency Alfvén-wave turbulence in the solar wind. *Astrophys J* 720:503–515. <https://doi.org/10.1088/0004-637X/720/1/503>
- Chandran BDG, Schekochihin AA, Mallet A (2015) Intermittency and alignment in strong RMHD turbulence. *Astrophys J* 807:39. <https://doi.org/10.1088/0004-637X/807/1/39>
- Chasapis A, Matthaeus WH, Parashar TN, Le Contel O, Retinò A, Breuillard H, Khotyaintsev Y, Vaivads A, Lavraud B, Eriksson E, Moore TE, Burch JL, Torbert RB, Lindqvist P-A, Ergun RE, Marklund G, Goodrich KA, Wilder FD, Chutter M, Needell J, Rau D, Dors I, Russell CT, Le G, Magnes W, Strangeway RJ, Bromund KR, Leinweber HK, Plaschke F, Fischer D, Anderson BJ, Pollock CJ, Giles BL, Paterson WR, Dorelli J, Gershman DJ, Avanov L, Saito Y (2017) Electron heating at kinetic scales in magnetosheath turbulence. *Astrophys J* 836(2):247. <https://doi.org/10.3847/1538-4357/836/2/247>
- Chasapis A, Matthaeus WH, Bandyopadhyay R, Chhiber R, Ahmadi N, Ergun RE, Russell CT, Strangeway RJ, Giles BL, Gershman DJ, Pollock CJ, Burch JL (2020) Scaling and anisotropy of solar wind turbulence at kinetic scales during the MMS turbulence campaign. *Astrophys J* 903(2):127. <https://doi.org/10.3847/1538-4357/abb948>
- Chen CHK, Mallet A, Yousef TA, Schekochihin AA, Horbury TS (2011) Anisotropy of Alfvénic turbulence in the solar wind and numerical simulations. *Mon Not R Astron Soc* 415:3219–3226. <https://doi.org/10.1111/j.1365-2966.2011.18933.x>
- Chen CHK, Mallet A, Schekochihin AA, Horbury TS, Wicks RT, Bale SD (2012) Three-dimensional structure of solar wind turbulence. *Astrophys J* 758:120. <https://doi.org/10.1088/0004-637X/758/2/120>
- Chen CHK, Leung L, Boldyrev S, Maruca BA, Bale SD (2014) Ion-scale spectral break of solar wind turbulence at high and low beta. *Geophys Res Lett* 41:8081–8088. <https://doi.org/10.1002/2014GL062009>
- Chen CHK (2016) Recent progress in astrophysical plasma turbulence from solar wind observations. *J Plasma Phys* 82:535820602. <https://doi.org/10.1017/S0022377816001124>
- Chen L-J, Bessho N, Bookbinder JA, Caprioli D, Goldstein M, Ji H, Jian LK, Karimabadi H, Khotyaintsev Y, Klein KG, Lavraud B, Matthaeus W, Moore TE, Retino A, Roberts OW, Roytershteyn V, Schiff C, Spence H, Stawarz J, TenBarge J, Wang S (2019) Challenges and the next transformative steps in understanding plasma turbulence from the perspective of multi-spacecraft measurements
- Chhiber R, Matthaeus WH, Bowen TA, Bale SD (2021) Subproton-scale intermittency in near-sun solar wind turbulence observed by the Parker solar probe. *Astrophys J Lett* 911(1):7. <https://doi.org/10.3847/2041-8213/abf04e>
- Coburn JT, Smith CW, Vasquez BJ, Stawarz JE, Forman MA (2012) The turbulent cascade and proton heating in the solar wind during solar minimum. *Astrophys J* 754(2):93. <https://doi.org/10.1088/0004-637X/754/2/93>
- Cornilleau-Wehrin N, Chanteur G, Perraut S, Rezeau L, Robert P, Roux A, de Villedary C, Canu P, Maksimovic M, de Conchy Y, Lacombe DHC, Lefeuvre F, Parrot M, Pinçon JL, Décréau PME, Harvey CC, Louarn P, Santolik O, Alleyne HSC, Roth M, Chust T, Le Contel O (2003) Staff team: first results obtained by the cluster STAFF experiment. *Ann Geophys* 21(2):437–456. <https://doi.org/10.5194/angeo-21-437-2003>
- Cranmer SR, van Ballegoijen AA (2012) Proton, electron, and ion heating in the fast solar wind from nonlinear coupling between Alfvénic and fast-mode turbulence. *Astrophys J* 754:92. <https://doi.org/10.1088/0004-637X/754/2/92>
- Dalena S, Rappazzo AF, Dmitruk P, Greco A, Matthaeus WH (2014) Test-particle acceleration in a hierarchical three-dimensional turbulence model. *Astrophys J* 783(2):143. <https://doi.org/10.1088/0004-637X/783/2/143>
- Dasso S, Milano LJ, Matthaeus WH, Smith CW (2005) Anisotropy in fast and slow solar wind fluctuations. *Astrophys J* 635(2):181–184. <https://doi.org/10.1086/499559>
- Davidson PA (2001) *An introduction to magnetohydrodynamics*. Cambridge texts in applied mathematics. Cambridge University Press, Cambridge. <https://doi.org/10.1017/CBO9780511626333>

- Davis N, Chandran BDG, Bowen TA, Badman ST, Dudok de Wit T, Chen CHK, Bale SD, Huang Z, Sioulas N, Velli M (2023) The evolution of the 1/f range within a single fast-solar-wind stream between 17.4 and 45.7 solar radii. <https://doi.org/10.48550/arXiv.2303.01663>
- DeForest CE, Killough R, Gibson S, Henry A, Case T, Beasley M, Laurent G, Colaninno R, Waltham N (2022) Polarimeter to UNify the Corona and Heliosphere (PUNCH): Science, Status, and Path to Flight. In: IEEE Aerospace Conference (AERO), pp 1–11 <https://doi.org/10.1109/AERO53065.2022.9843340>
- Dmitruk P, Matthaeus WH, Seenu N (2004) Test particle energization by current sheets and nonuniform fields in magnetohydrodynamic turbulence. *Astrophys J* 617:667–679. <https://doi.org/10.1086/425301>
- Dong C, Wang L, Huang Y-M, Comisso L, Sandstrom TA, Bhattacharjee A (2022) Reconnection-driven energy cascade in magnetohydrodynamic turbulence. *Sci Adv* 8(49):7627. <https://doi.org/10.1126/sciadv.abn7627>
- Dudok de Wit T (2004) Can high-order moments be meaningfully estimated from experimental turbulence measurements? *Phys Rev E* 70:055302. <https://doi.org/10.1103/PhysRevE.70.055302>
- Dudok de Wit T, Alexandrova O, Furno I, Sorriso-Valvo L, Zimbaro G (2013) Methods for characterising microphysical processes in plasmas. *Space Sci Rev* 178(2–4):665–693. <https://doi.org/10.1007/s11214-013-9974-9>
- Dunlop MW, Balogh A, Glassmeier K-H (2002a) Four-point Cluster application of magnetic field analysis tools: the discontinuity analyzer. *J Geophys Res Space Phys* 107(A11):1385. <https://doi.org/10.1029/2001JA005089>
- Dunlop MW, Balogh A, Glassmeier K-H, Robert P (2002b) Four-point Cluster application of magnetic field analysis tools: the Curlometer. *J Geophys Res Space Phys* 107(A11):1384. <https://doi.org/10.1029/2001JA005088>
- Dunlop MW, Dong X-C, Wang T-Y, Eastwood JP, Robert P, Haaland S, Yang Y-Y, Escoubet P, Rong Z-J, Shen C, Fu H-S, De Keyser J (2021) Curlometer technique and applications. *J Geophys Res Space Phys* 126(11):29538. <https://doi.org/10.1029/2021JA029538>
- Eastwood JP, Lucek EA, Mazelle C, Meziane K, Narita Y, Pickett J, Treumann RA (2005) The foreshock. *Space Sci Rev* 118(1–4):41–94. <https://doi.org/10.1007/s11214-005-3824-3>
- Elmegreen BG, Scalo J (2004) Interstellar turbulence I: observations and processes. *Annu Rev Astron Astrophys* 42(1):211–273. <https://doi.org/10.1146/annurev.astro.41.011802.094859>
- Elsasser WM (1950) The hydromagnetic equations. *Phys Rev* 79:183–183. <https://doi.org/10.1103/PhysRev.79.183>
- Escoubet CP, Fehring M, Goldstein M (2001) Introduction: the Cluster mission. *Ann Geophys* 19:1197–1200. <https://doi.org/10.5194/angeo-19-1197-2001>
- Escoubet CP, Masson A, Laakso H, Goldstein ML, Dimbylow T, Bogdanova YV, Hapgood M, Sousa B, Sieg D, Taylor MGGT (2021) Cluster after 20 years of operations: science highlights and technical challenges. *J Geophys Res Space Phys* 126(8):29474. <https://doi.org/10.1029/2021JA029474>
- Fischer D, Magnes W, Hagen C, Dors I, Chutter MW, Needell J, Torbert RB, Le Contel O, Strangeway RJ, Kubin G, Valavanoglou A, Plaschke F, Nakamura R, Mirioni L, Russell CT, Leinweber HK, Bromund KR, Le G, Kepko L, Anderson BJ, Slavin JA, Baumjohann W (2016) Optimized merging of search coil and fluxgate data for MMS. *Geosci Instrum Method Data Syst* 5(2):521–530. <https://doi.org/10.5194/gi-5-521-2016>
- Forest CB, Flanagan K, Brookhart M, Clark M, Cooper CM, Désangles V, Egedal J, Endrizzi D, Khalzov IV, Li H et al (2015) The Wisconsin Plasma Astrophysics Laboratory. *J Plasma Phys* 81(5):345810501. <https://doi.org/10.1017/S0022377815000975>
- Formisano V (1979) The three-dimensional shape of the bow shock. *Il Nuovo Cimento C* 2:681–692. <https://doi.org/10.1007/BF02558125>
- Fox NJ, Velli MC, Bale SD, Decker R, Driesman A, Howard RA, Kasper JC, Kinnison J, Kusterer M, Lario D, Lockwood MK, McComas DJ, Raouafi NE, Szabo A (2015) The Solar Probe Plus mission: humanity’s first visit to our star. *Space Sci Rev* 204:7–48. <https://doi.org/10.1007/s11214-015-0211-6>
- Fredricks RW, Coroniti FV (1976) Ambiguities in the deduction of rest frame fluctuation spectrums from spectrums computed in moving frames. *J Geophys Res* 81:5591–5595. <https://doi.org/10.1029/JA081i031p05591>
- Gary SP, Jian LK, Broiles TW, Stevens ML, Podesta JJ, Kasper JC (2016) Ion-driven instabilities in the solar wind: wind observations of 19. *J Geophys Res* 121:30–41. <https://doi.org/10.1002/2015JA021935>
- Gekelman W, Pribyl P, Lucky Z, Drandell M, Leneman D, Maggs J, Vincena S, Van Compernelle B, Tripathi SKP, Morales G (2016) The upgraded large plasma device, a machine for studying frontier basic plasma physics. *Rev Sci Instrum* 87(2):025105. <https://doi.org/10.1063/1.4941079>
- Ghosh S, Matthaeus WH, Roberts DA, Goldstein ML (1998) The evolution of slab fluctuations in the presence of pressure-balanced magnetic structures and velocity shears. *J Geophys Res* 103(A10):23691–23704. <https://doi.org/10.1029/98JA02195>

- Goldstein ML, Burlaga LF, Matthaeus WH (1984) Power spectral signatures of interplanetary corotating and transient flows. *J Geophys Res* 89(A6):3747–3761. <https://doi.org/10.1029/JA089iA06p03747>
- Goldstein ML, Roberts DA, Fitch CA (1994) Properties of the fluctuating magnetic helicity in the inertial and dissipation ranges of solar wind turbulence. *J Geophys Res* 99:11519–11538. <https://doi.org/10.1029/94JA00789>
- Grappin R, Velli M, Mangeney A (1993) Nonlinear wave evolution in the expanding solar wind. *Phys Rev Lett* 70(14):2190–2193. <https://doi.org/10.1103/PhysRevLett.70.2190>
- Grauer R, Krug J, Marliani C (1994) Scaling of high-order structure functions in magnetohydrodynamic turbulence. *Phys Lett A* 195(5–6):335–338. [https://doi.org/10.1016/0375-9601\(94\)90038-8](https://doi.org/10.1016/0375-9601(94)90038-8)
- Greco A, Matthaeus WH, Servidio S, Dmitruk P (2009) Waiting-time distributions of magnetic discontinuities: clustering or Poisson process? *Phys Rev E* 80(4):046401. <https://doi.org/10.1103/PhysRevE.80.046401>
- Greco A, Servidio S, Matthaeus WH, Dmitruk P (2010) Intermittent structures and magnetic discontinuities on small scales in MHD simulations and solar wind. *Planet Space Sci* 58:1895–1899. <https://doi.org/10.1016/j.pss.2010.08.019>
- Greco A, Matthaeus WH, D'Amicis R, Servidio S, Dmitruk P (2012) Evidence for nonlinear development of magnetohydrodynamic scale intermittency in the inner heliosphere. *Astrophys J* 749(2):105. <https://doi.org/10.1088/0004-637X/749/2/105>
- Grošelj D, Chen CHK, Mallet A, Samtaney R, Schneider K, Jenko F (2019) Kinetic turbulence in astrophysical plasmas: waves and/or structures? *Phys Rev X* 9(3):031037. <https://doi.org/10.1103/PhysRevX.9.031037>
- Hadid LZ, Sahraoui F, Galtier S (2017) Energy cascade rate in compressible fast and slow solar wind turbulence. *Astrophys J* 838(1):9. <https://doi.org/10.3847/1538-4357/aa603f>
- Hadid LZ, Sahraoui F, Galtier S, Huang SY (2018) Compressible magnetohydrodynamic turbulence in the Earth's magnetosheath: estimation of the energy cascade rate using in situ spacecraft data. *Phys Rev Lett* 120(5):055102. <https://doi.org/10.1103/PhysRevLett.120.055102>
- Hamilton K, Smith CW, Vasquez BJ, Leamon RJ (2008) Anisotropies and helicities in the solar wind inertial and dissipation ranges at 1 AU. *J Geophys Res Space Phys* 113:1106. <https://doi.org/10.1029/2007JA012559>
- He J, Wang L, Tu C, Marsch E, Zong Q (2015) Evidence of Landau and cyclotron resonance between protons and kinetic waves in solar wind turbulence. *Astrophys J Lett* 800(2):31. <https://doi.org/10.1088/2041-8205/800/2/L31>
- Hietala H, Phan TD, Angelopoulos V, Oieroset M, Archer MO, Karlsson T, Plaschke F (2018) In situ observations of a magnetosheath high-speed jet triggering magnetopause reconnection. *Geophys Res Lett* 45(4):1732–1740. <https://doi.org/10.1002/2017GL076525>
- Hollweg JV, Isenberg PA (2002) Generation of the fast solar wind: a review with emphasis on the resonant cyclotron interaction. *J Geophys Res* 107:1147. <https://doi.org/10.1029/2001JA002070>
- Horbury TS (2000) Cluster II analysis of turbulence using correlation functions. In: Harris RA (ed) Cluster-II workshop multiscale/multipoint plasma measurements. ESA special publication, vol 449, p 89
- Horbury TS, Balogh A (1997) Structure function measurements of the intermittent MHD turbulent cascade. *Nonlinear Process Geophys* 4(3):185–199. <https://doi.org/10.5194/npg-4-185-1997>
- Horbury TS, Forman M, Oughton S (2008) Anisotropic scaling of magnetohydrodynamic turbulence. *Phys Rev Lett* 101(17):175005. <https://doi.org/10.1103/PhysRevLett.101.175005>
- Horbury TS, Wicks RT, Chen CHK (2012) Anisotropy in space plasma turbulence: solar wind observations. *Space Sci Rev* 172:325–342. <https://doi.org/10.1007/s11214-011-9821-9>
- Horbury TS, O'Brien H, Blazquez IC, Bendyk M, Brown P, Hudson R, Evans V, Oddy TM, Carr CM, Beek TJ, Cupido E, Bhattacharya S, Dominguez J-A, Matthews L, Myklebust VR, Whiteside B, Bale SD, Baumjohann W, Burgess D, Carbone V, Cargill P, Eastwood J, Erdos G, Fletcher L, Forsyth R, Giacalone J, Glassmeier K-H, Goldstein ML, Hoeksema T, Lockwood M, Magnes W, Maksimovic M, Marsch E, Matthaeus WH, Murphy N, Nakariakov VM, Owen CJ, Owens M, Rodriguez-Pacheco J, Richter I, Riley P, Russell CT, Schwartz S, Vainio R, Velli M, Vennerstrom S, Walsh R, Wimmer-Schweingruber RF, Zank G, Muller D, Zouganelis I, Walsh AP (2020) The Solar Orbiter magnetometer. *Astron Astrophys*, 642:A9. <https://doi.org/10.1051/0004-6361/201937257>
- Howes GG (2015) A dynamical model of plasma turbulence in the solar wind. *Philos Trans R Soc Lond Ser A* 373:20140145. <https://doi.org/10.1098/rsta.2014.0145>
- Huang Z, Sioulas N, Shi C, Velli M, Bowen T, Davis N, Chandran BDG, Kang N, Shi X, Huang J, Bale SD, Kasper JC, Larson DE, Livu R, Whittlesey PL, Rahmati A, Paulson K, Stevens M, Case AW, Dudok de Wit T, Malaspina DM, Bonnell JW, Goetz K, Harvey PR, MacDowall RJ (2023) New observations of solar wind 1/f turbulence spectrum from Parker Solar Probe. *Astrophys J Lett* 950:L8. <https://doi.org/10.3847/2041-8213/acd7f2>

- Iroshnikov PS (1963) Turbulence of a conducting fluid in a strong magnetic field. *Astron Zhurnal* 40:742. <https://adsabs.harvard.edu/full/1964SvA.....7..566I>
- Isaacs JJ, Tessein JA, Matthaeus WH (2015) Systematic averaging interval effects on solar wind statistics. *J Geophys Res Space Phys* 120(2):868–879. <https://doi.org/10.1002/2014JA020661>
- Jian LK, Wei HY, Russell CT, Luhmann JG, Klecker B, Omid N, Isenberg PA, Goldstein ML, Figueroa-Viñas A, Blanco-Cano X (2014) Electromagnetic waves near the proton cyclotron frequency: STEREO observations. *Astrophys J* 786(2):123. <https://doi.org/10.1088/0004-637X/786/2/123>
- Jian LK, Russell CT, Luhmann JG, Galvin AB (2018) STEREO observations of interplanetary coronal mass ejections in 2007–2016. *Astrophys J* 855(2):114. <https://doi.org/10.3847/1538-4357/aab189>
- Jian LK, Luhmann JG, Russell CT, Galvin AB (2019) Solar terrestrial relations observatory (STEREO) observations of stream interaction regions in 2007–2016: relationship with heliospheric current sheets, solar cycle variations, and dual observations. *Sol Phys* 294(3):31. <https://doi.org/10.1007/s11207-019-1416-8>
- Jokipii JR (1972) Fokker-Planck equations for charged-particle transport in random fields. *Astrophys J* 172:319. <https://doi.org/10.1086/151349>
- Joyner M, Plice L (2023) Active swarm resiliency in the HelioSwarm mission. Proceedings of the Small Satellite Conference. Weekday Session 2: Missions at Scale, 74. <https://digitalcommons.usu.edu/smallsat/2023/all2023/74/>
- Juno J, Hakim A, TenBarge J, Shi E, Dorland W (2018) Discontinuous Galerkin algorithms for fully kinetic plasmas. *J Comp Phys* 353:110–147. <https://doi.org/10.1016/j.jcp.2017.10.009>
- Karimabadi H, Roytershteyn V, Wan M, Matthaeus WH, Daughton W, Wu P, Shay M, Loring B, Borovsky J, Leonardis E, Chapman SC, Nakamura TKM (2013) Coherent structures, intermittent turbulence, and dissipation in high-temperature plasmas. *Phys Plasmas* 20(1):012303. <https://doi.org/10.1063/1.4773205>
- Kasper JC, Lazarus AJ, Gary SP (2008) Hot solar-wind helium: direct evidence for local heating by Alfvén-cyclotron dissipation. *Phys Rev Lett* 101(26):261103. <https://doi.org/10.1103/PhysRevLett.101.261103>
- Kasper JC, Maruca BA, Stevens ML, Zaslavsky A (2013) Sensitive test for ion-cyclotron resonant heating in the solar wind. *Phys Rev Lett* 110(9):091102. <https://doi.org/10.1103/PhysRevLett.110.091102>
- Kasper JC, Abiad R, Austin G, Balat-Pichelin M, Bale SD, Belcher JW, Berg P, Bergner H, Berthomier M, Bookbinder J, Brodu E, Caldwell D, Case AW, Chandran BDG, Cheimets P, Cirtain JW, Cranmer SR, Curtis DW, Daigneau P, Dalton G, Dasgupta B, DeTomaso D, Diaz-Aguado M, Djordjevic B, Donaskowski B, Effinger M, Florinski V, Fox N, Freeman M, Gallagher D, Gary SP, Gauron T, Gates R, Goldstein M, Golub L, Gordon DA, Gurnee R, Guth G, Halekas J, Hatch K, Heerikuisen J, Ho G, Hu Q, Johnson G, Jordan SP, Korreck KE, Larson D, Lazarus AJ, Li G, Livi R, Ludlam M, Maksimovic M, McFadden JP, Marchant W, Maruca BA, McComas DJ, Messina L, Mercer T, Park S, Peddie AM, Pogorelov N, Reinhart MJ, Richardson JD, Robinson M, Rosen I, Skoug RM, Slagle A, Steinberg JT, Stevens ML, Szabo A, Taylor ER, Tiu C, Turin P, Velli M, Webb G, Whittlesey P, Wright K, Wu ST, Zank G (2015) Solar Wind Electrons Alphas and Protons (SWEAP) investigation: design of the solar wind and coronal plasma instrument suite for Solar Probe Plus. *Space Sci Rev* 204:131–186. <https://doi.org/10.1007/s11214-015-0206-3>
- Kasper JC, Klein KG, Weber T, Maksimovic M, Zaslavsky A, Bale SD, Maruca BA, Stevens ML, Case AW (2017) A zone of preferential ion heating extends tens of solar radii from the sun. *Astrophys J* 849:126. <https://doi.org/10.3847/1538-4357/aa84b1>
- Kiyani KH, Osman KT, Chapman SC (2015) Dissipation and heating in solar wind turbulence: from the macro to the micro and back again. *Philos Trans R Soc Lond Ser A* 373(2041):20140155. <https://doi.org/10.1098/rsta.2014.0155>
- Klein KG, Vech D (2019) Solar wind plasma parameter distributions at 1 au. *Res Notes Am Astron Soc* 3(7):107. <https://doi.org/10.3847/2515-5172/ab3465>
- Klein KG, Howes GG, TenBarge JM, Bale SD, Chen CHK, Salem CS (2012) Using synthetic spacecraft data to interpret compressible fluctuations in solar wind turbulence. *Astrophys J* 755:159. <https://doi.org/10.1088/0004-637X/755/2/159>
- Klein KG, Howes GG, TenBarge JM (2014) The violation of the Taylor hypothesis in measurements of solar wind turbulence. *Astrophys J Lett* 790:20. <https://doi.org/10.1088/2041-8205/790/2/L20>
- Klein KG, Howes GG, TenBarge JM, Podesta JJ (2014) Physical interpretation of the angle dependent magnetic helicity spectrum in the slow wind: the nature of turbulent fluctuations near the proton gyroradius scale. *Astrophys J* 785:138. <https://doi.org/10.1088/0004-637X/785/2/138>
- Klein KG, Alexandrova O, Bookbinder J, Caprioli D, Case AW, Chandran BDG, Chen LJ, Horbury T, Jian L, Kasper JC, Le Contel O, Maruca BA, Matthaeus W, Retino A, Roberts O, Schekochihin A, Skoug R, Smith C, Steinberg J, Spence H, Vasquez B, TenBarge JM, Verscharen D, Whittlesey P (2019) [Plasma 2020 Decadal] Multipoint measurements of the solar wind: a proposed advance for studying magnetized turbulence. [arXiv:1903.05740](https://arxiv.org/abs/1903.05740)

- Kolmogorov A (1941) The local structure of turbulence in incompressible viscous fluid for very large Reynolds' numbers. *Akad. Nauk SSSR Doklady* 30:301–305
- Kolmogorov AN (1962) A refinement of previous hypotheses concerning the local structure of turbulence in a viscous incompressible fluid at high Reynolds number. *J Fluid Mech* 13:82–85. <https://doi.org/10.1017/S0022112062000518>
- Kraichnan RH (1965) Inertial-range spectrum of hydromagnetic turbulence. *Phys Fluids* 8:1385–1387. <https://doi.org/10.1063/1.1761412>
- Kulsrud RM (2005) *Plasma physics for astrophysics*. Princeton University Press. <https://doi.org/10.2307/j.ctvzsmf0w>
- Kulsrud RM, Zweibel EG (2008) On the origin of cosmic magnetic fields. *Rep Prog Phys* 71(4):046901. <https://doi.org/10.1088/0034-4885/71/4/046901>
- Kunz MW, Stone JM, Bai X-N (2014) Pegasus: a new hybrid-kinetic particle-in-cell code for astrophysical plasma dynamics. *J Comp Phys* 259:154–174. <https://doi.org/10.1016/j.jcp.2013.11.035>
- Kunz MW, Schekochihin AA, Chen CHK, Abel IG, Cowley SC (2015) Inertial-range kinetic turbulence in pressure-anisotropic astrophysical plasmas. *J Plasma Phys* 81(5):325810501. <https://doi.org/10.1017/S0022377815000811>
- Kunz MW, Abel IG, Klein KG, Schekochihin AA (2018) Astrophysical gyrokinetics: turbulence in pressure-anisotropic plasmas at ion scales and beyond. *J Plasma Phys* 84(2):715840201. <https://doi.org/10.1017/S0022377818000296>
- Kunz MW, Jones TW, Zhuravleva I (2022) Plasma physics of the intracluster medium. In: Bambi C, Santangelo A (eds) *Handbook of X-ray and gamma-ray astrophysics*. Springer, Singapore, pp 1–42. https://doi.org/10.1007/978-981-16-4544-0_125-1
- le Roux JA, Zank GP, Webb GM, Khabarova O (2015) A kinetic transport theory for particle acceleration and transport in regions of multiple contracting and reconnecting inertial-scale flux ropes. *Astrophys J* 801(2):112. <https://doi.org/10.1088/0004-637X/801/2/112>
- Leamon RJ, Smith CW, Ness NF, Wong HK (1999) Dissipation range dynamics: kinetic Alfvén waves and the importance of β_e . *J Geophys Res* 104:22331–22344. <https://doi.org/10.1029/1999JA900158>
- Levinson-Muth P, Dono A, Plice L (2021b) Eclipse mitigation strategies in p/2 lunar resonant orbits. In: *AAS/AIAA astrodynamics specialist conference*
- Levinson-Muth P, Plice L, Alvarelos J (2021a) Helioswarm: relative orbit maintenance in eccentric p/2 lunar resonant orbit. In: *AAS/AIAA astrodynamics specialist conference*
- Levinson-Muth P, West S, Plice L (2022) Helioswarm: swarm design methods in eccentric p/2 lunar resonant orbit. In: *AAS/AIAA astrodynamics specialist conference*
- Lion S, Alexandrova O, Zaslavsky A (2016) Coherent events and spectral shape at ion kinetic scales in the fast solar wind turbulence. *Astrophys J* 824(1):47. <https://doi.org/10.3847/0004-637X/824/1/47>
- Loto'aniu PTM, Romich K, Rowland W, Codrescu S, Biesecker D, Johnson J, Singer HJ, Szabo A, Stevens M (2022) Validation of the DSCOVR spacecraft mission space weather solar wind products. *Space Weather* 20(10):e2022SW003085. <https://doi.org/10.1029/2022SW003085>
- Loureiro NF, Boldyrev S (2017) Role of magnetic reconnection in magnetohydrodynamic turbulence. *Phys Rev Lett* 118(24):245101. <https://doi.org/10.1103/PhysRevLett.118.245101>
- Mac Low M-M, Ossenkopf V (2000) Characterizing the structure of interstellar turbulence. *Astron Astrophys* 353:339–348
- MacBride BT, Forman MA, Smith CW (2005) Turbulence and third moment of fluctuations: Kolmogorov's 4/5 law and its MHD analogues in the solar wind. In: Fleck B, Zurbuchen TH, Lacoste H (eds) *Solar wind 11/SOHO 16, Connecting sun and heliosphere*. ESA special publication, vol 592, p 613
- MacBride BT, Smith CW, Forman MA (2008) The turbulent cascade at 1 AU: energy transfer and the third-order scaling for MHD. *Astrophys J* 679:1644–1660. <https://doi.org/10.1086/529575>
- Mallet A, Schekochihin AA (2017) A statistical model of three-dimensional anisotropy and intermittency in strong Alfvénic turbulence. *Mon Not R Astron Soc* 466(4):3918–3927. <https://doi.org/10.1093/mnras/stw3251>
- Mallet A, Schekochihin AA, Chandran BDG (2015) Refined critical balance in strong Alfvénic turbulence. *Mon Not R Astron Soc* 449:77–81. <https://doi.org/10.1093/mnras/slv021>
- Mallet A, Schekochihin AA, Chandran BDG, Chen CHK, Horbury TS, Wicks RT, Greenan CC (2016) Measures of three-dimensional anisotropy and intermittency in strong Alfvénic turbulence. *Mon Not R Astron Soc* 459(2):2130–2139. <https://doi.org/10.1093/mnras/stw802>
- Mallet A, Schekochihin AA, Chandran BDG (2017) Disruption of sheet-like structures in Alfvénic turbulence by magnetic reconnection. *Mon Not R Astron Soc* 468(4):4862–4871. <https://doi.org/10.1093/mnras/stx670>
- Mallet A, Klein KG, Chandran BDG, Grošelj D, Hoppock IW, Bowen TA, Salem CS, Bale SD (2019) Interplay between intermittency and dissipation in collisionless plasma turbulence. *J Plasma Phys* 85(3):175850302. <https://doi.org/10.1017/S0022377819000357>

- Marsch E (2012) Helios: evolution of distribution functions 0.3-1 AU. *Space Sci Rev* 172:23–39. <https://doi.org/10.1007/s11214-010-9734-z>
- Maruca BA, Chasapis A, Gary SP, Bandyopadhyay R, Chhiber R, Parashar TN, Matthaeus WH, Shay MA, Burch JL, Moore TE, Pollock CJ, Giles BJ, Paterson WR, Dorelli J, Gershman DJ, Torbert RB, Russell CT, Strangeway RJ (2018) MMS observations of beta-dependent constraints on ion temperature anisotropy in Earth's magnetosheath. *Astrophys J* 866(1):25. <https://doi.org/10.3847/1538-4357/aaddfb>
- Matthaeus WH (2021) Turbulence in space plasmas: who needs it? *Phys Plasmas* 28(3):032306. <https://doi.org/10.1063/5.0041540>
- Matthaeus WH, Goldstein ML (1982) Stationarity of magnetohydrodynamic fluctuations in the solar wind. *J Geophys Res* 87:10347–10354. <https://doi.org/10.1029/JA087iA12p10347>
- Matthaeus WH, Lamkin SL (1986) Turbulent magnetic reconnection. *Phys Fluids* 29(8):2513–2534. <https://doi.org/10.1063/1.866004>
- Matthaeus WH, Velli M (2011) Who needs turbulence? A review of turbulence effects in the heliosphere and on the fundamental process of reconnection. *Space Sci Rev* 160:145–168. <https://doi.org/10.1007/s11214-011-9793-9>
- Matthaeus WH, Goldstein ML, Roberts DA (1990) Evidence for the presence of quasi-two-dimensional nearly incompressible fluctuations in the solar wind. *J Geophys Res* 95:20673–20683. <https://doi.org/10.1029/JA095iA12p20673>
- Matthaeus WH, Zank GP, Oughton S, Mullan DJ, Dmitruk P (1999) Coronal heating by magnetohydrodynamic turbulence driven by reflected low-frequency waves. *Astrophys J Lett* 523:93–96. <https://doi.org/10.1086/312259>
- Matthaeus WH, Dasso S, Weygand JM, Milano LJ, Smith CW, Kivelson MG (2005) Spatial correlation of solar-wind turbulence from two-point measurements. *Phys Rev Lett* 95(23):231101. <https://doi.org/10.1103/PhysRevLett.95.231101>
- Matthaeus WH, Breech B, Dmitruk P, Bemporad A, Poletto G, Velli M, Romoli M (2007) Density and magnetic field signatures of interplanetary 1/f noise. *Astrophys J* 657(2):121–124. <https://doi.org/10.1086/513075>
- Matthaeus WH, Wan M, Servidio S, Greco A, Osman KT, Oughton S, Dmitruk P (2015) Intermittency, nonlinear dynamics and dissipation in the solar wind and astrophysical plasmas. *Philos Trans R Soc Lond Ser A* 373:20140154. <https://doi.org/10.1098/rsta.2014.0154>
- Matthaeus WH, Parashar TN, Wan M, Wu P (2016) Turbulence and proton-electron heating in kinetic plasma. *Astrophys J* 827(1):7. <https://doi.org/10.3847/2041-8205/827/1/L7>
- Matthaeus WH, Weygand JM, Dasso S (2016) Ensemble space-time correlation of plasma turbulence in the solar wind. *Phys Rev Lett* 116(24):245101. <https://doi.org/10.1103/PhysRevLett.116.245101>
- Matthaeus WH, Bandyopadhyay R, Brown MR, Borovsky J, Carbone V, Caprioli D, Chasapis A, Chhiber R, Dasso S, Dmitruk P, Del Zanna L, Dmitruk PA, Franci L, Gary SP, Goldstein ML, Gomez D, Greco A, Horbury TS, Ji H, Kasper JC, Klein KG, Landi S, Li H, Malara F, Maruca BA, Mininni P, Oughton S, Papini E, Parashar TN, Petrosyan A, Pouquet A, Retino A, Roberts O, Ruffolo D, Servidio S, Spence H, Smith CW, Stawarz JE, TenBarge J, Vasquez BJ, Vaivads A, Valentini F, Velli M, Verdini A, Verscharen D, Whittlesey P, Wicks R, Bruno R, Zimbardo G (2019) [Plasma 2020 Decadal] The essential role of multi-point measurements in turbulence investigations: the solar wind beyond single scale and beyond the Taylor hypothesis. [arXiv:1903.06890](https://arxiv.org/abs/1903.06890)
- McComas DJ, Christian ER, Schwadron NA, Fox N, Westlake J, Allegrini F, Baker DN, Biesecker D, Bzowski M, Clark G, Cohen CMS, Cohen I, Dayeh MA, Decker R, de Nolfo GA, Desai MI, Ebert RW, Elliott HA, Fahr H, Frisch PC, Funsten HO, Fuselier SA, Galli A, Galvin AB, Giacalone J, Gkioulidou M, Guo F, Horanyi M, Isenberg P, Janzen P, Kistler LM, Korreck K, Kubiak MA, Kucharek H, Larsen BA, Leske RA, Lugaz N, Luhmann J, Matthaeus W, Mitchell D, Moebius E, Ogasawara K, Reisenfeld DB, Richardson JD, Russell CT, Sokol JM, Spence HE, Skoug R, Sternovsky Z, Swaczyna P, Szalay JR, Tokumaru M, Wiedenbeck ME, Wurz P, Zank GP, Zirnstein EJ (2018) Interstellar Mapping And Acceleration Probe (IMAP): a new NASA mission. *Space Sci Rev* 214(8):116. <https://doi.org/10.1007/s11214-018-0550-1>
- McFadden JP, Carlson CW, Larson D, Ludlam M, Abiad R, Elliott B, Turin P, Marckwordt M, Angelopoulos V (2008) The THEMIS ESA plasma instrument and in-flight calibration. *Space Sci Rev* 141(1–4):277–302. <https://doi.org/10.1007/s11214-008-9440-2>
- McKee CF, Ostriker EC (2007) Theory of star formation. *Annu Rev Astron Astrophys* 45(1):565–687. <https://doi.org/10.1146/annurev.astro.45.051806.110602>
- Meyrand R, Squire J, Schekochihin AA, Dorland W (2021) On the violation of the zeroth law of turbulence in space plasmas. *J Plasma Phys* 87(3):535870301. <https://doi.org/10.1017/S0022377821000489>
- Moffatt K, Dormy E (2019) Self-exciting fluid dynamos. Cambridge texts in applied mathematics. Cambridge University Press. <https://doi.org/10.1017/9781107588691>

- Montgomery D, Armstrong JW, Barnes A, Burke JD, Burlaga LF, Gary SP, Goldstein M, Gurnett DA, Jokipii JR, Kelley MC, Kintner P, Maggs JE, Morse F, Newton GP, Schulz M, Smith EJ, Sonett CP, Temerin M, Tsurutani BT, Uphoff CW, Wallace RA, Woo RT (1980) Report of the NASA plasma turbulence explorer study group. Technical Report 715-78, Jet Propulsion Laboratory, Pasadena, CA
- Müller D, Marsden RG, St. Cyr OC, Gilbert HR (2013) Solar orbiter. Exploring the sun-heliosphere connection. *Sol Phys* 285:25–70. <https://doi.org/10.1007/s11207-012-0085-7>
- Müller D, St. Cyr OC, Zouganelis I, Gilbert HR, Marsden R, Nieves-Chinchilla T, Antonucci E, Auchère F, Berghmans D, Horbury TS, Howard RA, Krucker S, Maksimovic M, Owen CJ, Rochus P, Rodriguez-Pacheco J, Romoli M, Solanki SK, Bruno R, Carlsson M, Fludra A, Harra L, Hassler DM, Livi S, Louarn P, Peter H, Schühle U, Teriaca L, del Toro Iniesta JC, Wimmer-Schweingruber RF, Marsch E, Velli M, De Groof A, Walsh A, Williams D (2020) The Solar Orbiter mission. Science overview. *Astron Astrophys* 642:1. <https://doi.org/10.1051/0004-6361/202038467>
- Narita Y, Glassmeier K-H, Motschmann U (2022) The wave telescope technique. *J Geophys Res Space Phys* 127(2):2021–030165. <https://doi.org/10.1029/2021JA030165>
- NASA (2014) Our dynamic space environment: heliophysics science and technology roadmap for 2014–2033. <https://science.nasa.gov/heliophysics/resources/>
- National Research Council (2013) Solar and space physics: a science for a technological society. The National Academies Press, Washington. <https://doi.org/10.17226/13060>. <https://www.nap.edu/catalog/13060/solar-and-space-physics-a-science-for-a-technological-society>
- Nelkin M, Tabor M (1990) Time correlations and random sweeping in isotropic turbulence. *Phys Fluids A* 2(1):81–83. <https://doi.org/10.1063/1.857684>
- Neugebauer M (1976) The role of Coulomb collisions in limiting differential flow and temperature differences in the solar wind. *J Geophys Res* 81(1):78. <https://doi.org/10.1029/JA081i001p00078>
- Ogilvie KW, Chornay DJ, Fritzenreiter RJ, Hunsaker F, Keller J, Lobell J, Miller G, Scudder JD, Sittler EC Jr, Torbert RB, Bodet D, Needell G, Lazarus AJ, Steinberg JT, Tappan JH, Mavretic A, Gergin E (1995) SWE, a comprehensive plasma instrument for the wind spacecraft. *Space Sci Rev* 71:55–77. <https://doi.org/10.1007/BF00751326>
- Orszag SA, Patterson GS (1972) Numerical simulation of three-dimensional homogeneous isotropic turbulence. *Phys Rev Lett* 28(2):76–79. <https://doi.org/10.1103/PhysRevLett.28.76>
- Osman KT, Horbury TS (2007) Multispacecraft measurement of anisotropic correlation functions in solar wind turbulence. *Astrophys J Lett* 654(1):103–106. <https://doi.org/10.1086/510906>
- Osman KT, Matthaeus WH, Greco A, Servidio S (2011) Evidence for inhomogeneous heating in the solar wind. *Astrophys J Lett* 727:11. <https://doi.org/10.1088/2041-8205/727/1/L11>
- Osman KT, Wan M, Matthaeus WH, Weygand JM, Dasso S (2011) Anisotropic third-moment estimates of the energy cascade in solar wind turbulence using multispacecraft data. *Phys Rev Lett* 107(16):165001. <https://doi.org/10.1103/PhysRevLett.107.165001>
- Oughton S, Matthaeus WH, Dmitruk P (2017) Reduced MHD in astrophysical applications: two-dimensional or three-dimensional? *Astrophys J* 839(1):2. <https://doi.org/10.3847/1538-4357/aa67e2>
- Owen CJ, Bruno R, Livi S, Louarn P, Al Janabi K, Allegrini F, Amoros C, Baruah R, Barthe A, Berthomier M, Bordon S, Brockley-Blatt C, Brysbaert C, Capuano G, Collier M, DeMarco R, Fedorov A, Ford J, Fortunato V, Fratter I, Galvin AB, Hancock B, Heirtzler D, Kataria D, Kistler L, Lepri ST, Lewis G, Loeffler C, Marty W, Mathon R, Mayall A, Mele G, Ogasawara K, Orlandi M, Pacros A, Penou E, Persyn S, Petiot M, Phillips M, Přečhl L, Raines JM, Reden M, Rouillard AP, Rousseau A, Rubiella J, Seran H, Spencer A, Thomas JW, Trevino J, Verscharen D, Wurz P, Alapide A, Amoroso L, André N, Anekallu C, Arciuli V, Arnett KL, Ascolese R, Bancroft C, Bland P, Brysch M, Calvanese R, Castronuovo M, Čermák I, Chornay D, Clemens S, Coker J, Collinson G, D'Amicis R, Dandouras I, Darnley R, Davies D, Davison G, De Los Santos A, Devoto P, Dirks G, Edlund E, Fazakerley A, Ferris M, Frost C, Fruit G, Garat C, Génou V, Gibson W, Gilbert JA, de Giosa V, Gradone S, Hailey M, Horbury TS, Hunt T, Jacquy C, Johnson M, Lavraud B, Lawrenson A, Leblanc F, Lockhart W, Maksimovic M, Malpus A, Maruccci F, Mazelle C, Monti F, Myers S, Nguyen T, Rodriguez-Pacheco J, Phillips I, Popecki M, Rees K, Rogacki SA, Ruane K, Rust D, Salatti M, Sauvaud JA, Stakhiv MO, Stange J, Stubbs T, Taylor T, Techer J-D, Terrier G, Thibodeaux R, Urdiales C, Varsani A, Walsh AP, Watson G, Wheeler P, Willis G, Wimmer-Schweingruber RF, Winter B, Yardley J, Zouganelis I (2020) The Solar Orbiter Solar Wind Analyser (SWA) suite. *Astron Astrophys* 642:16. <https://doi.org/10.1051/0004-6361/201937259>
- Parashar TN, Salem C, Wicks RT, Karimabadi H, Gary SP, Matthaeus WH (2015) Turbulent dissipation challenge: a community-driven effort. *J Plasma Phys* 81(5):905810513. <https://doi.org/10.1017/S0022377815000860>
- Parashar TN, Matthaeus WH, Shay MA (2018) Dependence of kinetic plasma turbulence on plasma β . *Astrophys J Lett* 864(1):21. <https://doi.org/10.3847/2041-8213/aadb8b>
- Parker EN (1979) Cosmical magnetic fields: their origin and their activity. International series of monographs on physics. Clarendon Press























- Paschmann G, Daly PW (1998) Analysis methods for multi-spacecraft data. ISSI scientific reports series, SR-001. ESA/ISSI. <https://www.issibern.ch/publications/issi-scientific-report-series/>
- Paschmann G, Daly PW (2008) Multi-spacecraft analysis methods revisited. ISSI scientific reports series, SR-008. ESA/ISSI. ISBN 978-92-9221-937-6
- Pecora F, Servidio S, Primavera L, Greco A, Yang Y, Matthaeus WH (2023) Multipoint turbulence analysis with helioswarm. *Astrophys J Lett* 945(2):20. <https://doi.org/10.3847/2041-8213/acbb03>
- Perri S, Valentini F, Sorriso-Valvo L, Reda A, Malara F (2017) On the estimation of the current density in space plasmas: multi-versus single-point techniques. *Planet Space Sci* 140:6–10. <https://doi.org/10.1016/j.pss.2017.03.008>
- Perrone D, Alexandrova O, Mangeney A, Maksimovic M, Lacombe C, Rakoto V, Kasper JC, Jovanovic D (2016) Compressive coherent structures at ion scales in the slow solar wind. *Astrophys J* 826(2):196. <https://doi.org/10.3847/0004-637X/826/2/196>
- Pinçon JL, Lefeuvre F (1991) Local characterization of homogeneous turbulence in a space plasma from simultaneous measurements of field components at several points in space. *J Geophys Res* 96:1789–1802. <https://doi.org/10.1029/90JA02183>
- Pitňa A, Šafránková J, Němeček Z, Franci L, Pi G (2021) A novel method for estimating the intrinsic magnetic field spectrum of kinetic-range turbulence. *Atmosphere* 12(12):1547. <https://doi.org/10.3390/atmos12121547>
- Plíce L, Perez AD, West SG (2019) HelioSwarm: swarm mission design in high altitude orbit for heliophysics. In: AAS/AIAA astrodynamics specialist conference. <https://ntrs.nasa.gov/citations/20190029108>
- Retinò A (2020) The search-coil magnetometer onboard the ESA JUICE mission. In: EGU general assembly conference abstracts, p 21172. <https://doi.org/10.5194/egusphere-egu2020-21172>
- Retinò A (2023) The Search-Coil Magnetometer (SCM) on the Jupiter ICy moons Explorer (JUICE) Radio & Plasma Wave Investigation (RPWI) instrument. *Space Sci Rev.* (to be submitted)
- Retinò A, Sundkvist D, Vaivads A, Mozer F, André M, Owen CJ (2007) In situ evidence of magnetic reconnection in turbulent plasma. *Nat Phys* 3(4):236–238. <https://doi.org/10.1038/nphys574>
- Richardson JD, Paularena KI, Lazarus AJ, Belcher JW (1995) Radial evolution of the solar wind from IMP 8 to Voyager 2. *Geophys Res Lett* 22(4):325–328. <https://doi.org/10.1029/94GL03273>
- Roberts OW, Li X, Jeska L (2015) A statistical study of the solar wind turbulence at ion kinetic scales using the k-filtering technique and cluster data. *Astrophys J* 802:2. <https://doi.org/10.1088/0004-637X/802/1/2>
- Roberts OW, Li X, Alexandrova O, Li B (2016) Observation of an MHD Alfvén vortex in the slow solar wind. *J Geophys Res Space Phys* 121(5):3870–3881. <https://doi.org/10.1002/2015JA022248>
- Roberts OW, Vörös Z, Torkar K, Stawarz J, Bandyopadhyay R, Gershman DJ, Narita Y, Kieokaew R, Lavraud B, Klein K, Yang Y, Nakamura R, Chasapis A, Matthaeus WH (2023) Estimation of the error in the calculation of the pressure-strain term: application in the terrestrial magnetosphere. *J Geophys Res Space Phys* 128:e2023JA031565. <https://doi.org/10.1029/2023JA031565>
- Roux A, Le Contel O, Coillot C, Bouabdellah A, de La Porte B, Alison D, Ruocco S, Vassal MC (2008) The search coil magnetometer for THEMIS. *Space Sci Rev* 141(1–4):265–275. <https://doi.org/10.1007/s11214-008-9455-8>
- Sahraoui F, Belmont G, Goldstein ML, Rezeau L (2010b) Limitations of multispacecraft data techniques in measuring wave number spectra of space plasma turbulence. *J Geophys Res* 115:4206. <https://doi.org/10.1029/2009JA014724>
- Sahraoui F, Goldstein ML, Belmont G, Canu P, Rezeau L (2010a) Three dimensional anisotropic k spectra of turbulence at subproton scales in the solar wind. *Phys Rev Lett* 105(13):131101. <https://doi.org/10.1103/PhysRevLett.105.131101>
- Sanada T, Shanmugasundaram V (1992) Random sweeping effect in isotropic numerical turbulence. *Phys Fluids A* 4(6):1245–1250. <https://doi.org/10.1063/1.858242>
- Scalo J, Elmegreen BG (2004) Interstellar turbulence II: implications and effects. *Annu Rev Astron Astrophys* 42(1):275–316. <https://doi.org/10.1146/annurev.astro.42.120403.143327>
- Schekochihin AA (2022) MHD turbulence: a biased review. *J Plasma Phys* 88(5):155880501. <https://doi.org/10.1017/S0022377822000721>
- Schekochihin AA, Cowley SC, Dorland W, Hammett GW, Howes GG, Quataert E, Tatsuno T (2009) Astrophysical gyrokinetics: kinetic and fluid turbulent cascades in magnetized weakly collisional plasmas. *Astrophys J Supp* 182:310–377. <https://doi.org/10.1088/0067-0049/182/1/310>
- Schwartz SJ, Horbury T, Owen C, Baumjohann W, Nakamura R, Canu P, Roux A, Sahraoui F, Louarn P, Sauvaud J-A, Pinçon J-L, Vaivads A, Marcucci MF, Anastasiadis A, Fujimoto M, Escoubet P, Taylor M, Eckersley S, Allouis E, Perkinson M-C (2009) Cross-scale: multi-scale coupling in space plasmas. *Exp Astron* 23(3):1001–1015. <https://doi.org/10.1007/s10686-008-9085-x>
- Servidio S, Carbone V, Dmitruk P, Matthaeus WH (2011) Time decorrelation in isotropic magnetohydrodynamic turbulence. *Europhys Lett* 96(5):55003. <https://doi.org/10.1209/0295-5075/96/55003>

- Smith EJ, Marsden RG, Page DE (1995) Ulysses above the sun's south pole: an introduction. *Science* 268:1005–1007. <https://doi.org/10.1126/science.7754377>
- Smith CW, Vasquez BJ, Coburn JT, Forman MA, Stawarz JE (2018) Correlation scales of the turbulent cascade at 1 au. *Astrophys J* 858(1):21. <https://doi.org/10.3847/1538-4357/aabb00>
- Squire J, Meyrand R, Kunz MW, Arzamasskiy L, Schekochihin AA, Quataert E (2022) High-frequency heating of the solar wind triggered by low-frequency turbulence. *Nat Astron*. <https://doi.org/10.1038/s41550-022-01624-z>
- Sreenivasan KR, Antonia RA (1997) The phenomenology of small-scale turbulence. *Annu Rev Fluid Mech* 29:435–472. <https://doi.org/10.1146/annurev.fluid.29.1.435>
- Stawarz JE, Smith CW, Vasquez BJ, Forman MA, MacBride BT (2009) The turbulent cascade and proton heating in the solar wind at 1 AU. *Astrophys J* 697(2):1119–1127. <https://doi.org/10.1088/0004-637X/697/2/1119>
- Stawarz JE, Eastwood JP, Phan TD, Gingell IL, Pyakurel PS, Shay MA, Robertson SL, Russell CT, Le Contel O (2022) Turbulence-driven magnetic reconnection and the magnetic correlation length: observations from magnetospheric multiscale in Earth's magnetosheath. *Phys Plasmas* 29(1):012302. <https://doi.org/10.1063/5.0071106>
- Stone EC, Frandsen AM, Mewaldt RA, Christian ER, Margolies D, Ormes JF, Snow F (1998) The advanced composition explorer. *Space Sci Rev* 86:1–22. <https://doi.org/10.1023/A:1005082526237>
- Takahashi K, Lee D-H, Merkin VG, Lyon JG, Hartinger MD (2016) On the origin of the dawn-dusk asymmetry of toroidal Pc5 waves. *J Geophys Res Space Phys* 121(10):9632–9650. <https://doi.org/10.1002/2016JA023009>
- Taylor GI (1935) Statistical theory of turbulence. *Proc R Soc Lond Ser A* 151(873):421–444. <https://doi.org/10.1098/rspa.1935.0158>
- Taylor GI (1938) The spectrum of turbulence. *Proc R Soc Lond A* 164:476–490. <https://doi.org/10.1098/rspa.1938.0032>
- TenBarge JM, Howes GG (2013) Current sheets and collisionless damping in kinetic plasma turbulence. *Astrophys J Lett* 771:27. <https://doi.org/10.1088/2041-8205/771/2/L27>
- TenBarge JM, Alexandrova O, Boldyrev S, Califano F, Cerri SS, Chen CHK, Howes GG, Horbury T, Isenberg PA, Ji H, Klein KG, Krafft C, Kunz M, Loureiro NF, Mallet A, Maruca BA, Matthaeus WH, Meyrand R, Quataert E, Perez JC, Roberts OW, Sahraoui F, Salem CS, Schekochihin AA, Spence H, Squire J, Told D, Verscharen D, Wicks RT (2019) [Plasma 2020 Decadal] Disentangling the spatiotemporal structure of turbulence using multi-spacecraft data. [arXiv:1903.05710](https://arxiv.org/abs/1903.05710)
- Tennekes H (1975) Eulerian and Lagrangian time microscales in isotropic turbulence. *J Fluid Mech* 67:561–567. <https://doi.org/10.1017/S0022112075000468>
- Toepfer S, Glassmeier K-H, Motschmann U (2023) Concerning the detection of electromagnetic knot structures in space plasmas using the wave telescope technique. *Ann Geophys* 41:253–267. <https://doi.org/10.5194/angeo-41-253-2023>
- Vech D, Klein KG, Kasper JC (2017) Nature of stochastic ion heating in the solar wind: testing the dependence on plasma beta and turbulence amplitude. *Astrophys J Lett* 850(1):11. <https://doi.org/10.3847/2041-8213/aa9887>
- Vech D, Mallet A, Klein KG, Kasper JC (2018) Magnetic reconnection may control the ion-scale spectral break of solar wind turbulence. *Astrophys J Lett* 855(2):27. <https://doi.org/10.3847/2041-8213/aab351>
- Verdini A, Velli M, Matthaeus WH, Oughton S, Dmitruk P (2010) A turbulence-driven model for heating and acceleration of the fast wind in coronal holes. *Astrophys J* 708(2):116–120. <https://doi.org/10.1088/2041-8205/708/2/L116>
- Verscharen D, Klein KG, Maruca BA (2019) The multi-scale nature of the solar wind. *Living Rev Sol Phys* 16(1):5. <https://doi.org/10.1007/s41116-019-0021-0>
- Völk HJ, Alpers W (1972) Spectral anisotropy of Alfvén-waves in the solar wind. In: Schindler K (ed) *Cosmic plasma physics*. Springer, Boston, MA, p 105–111. https://doi.org/10.1007/978-1-4615-6758-5_14
- Wan M, Matthaeus WH, Roytershteyn V, Parashar TN, Wu P, Karimabadi H (2016) Intermittency, coherent structures and dissipation in plasma turbulence. *Phys Plasmas* 23(4):042307. <https://doi.org/10.1063/1.4945631>
- Wang L, Hakim AH, Bhattacharjee A, Germaschewski K (2015) Comparison of multi-fluid moment models with particle-in-cell simulations of collisionless magnetic reconnection. *Phys Plasmas* 22(1):012108. <https://doi.org/10.1063/1.4906063>
- Wang T, Alexandrova O, Perrone D, Dunlop M, Dong X, Bingham R, Khotyaintsev YV, Russell CT, Giles BL, Torbert RB, Ergun RE, Burch JL (2019) Magnetospheric multiscale observation of kinetic signatures in the Alfvén vortex. *Astrophys J Lett* 871(2):22. <https://doi.org/10.3847/2041-8213/aafe0d>
- Weygand JM, Matthaeus WH, Dasso S, Kivelson MG, Kistler LM, Moukikis C (2009) Anisotropy of the Taylor scale and the correlation scale in plasma sheet and solar wind magnetic field fluctuations. *J Geophys Res Space Phys* 114(A7):07213. <https://doi.org/10.1029/2008JA013766>

- Whittlesey PL, Larson DE, Kasper JC, Halekas J, Abatcha M, Abiad R, Berthomier M, Case AW, Chen J, Curtis DW, Dalton G, Klein KG, Korreck KE, Livi R, Ludlam M, Marckwordt M, Rahmati A, Robinson M, Slagle A, Stevens ML, Tiu C, Verniero JL (2020) The Solar Probe ANalyzers—Electrons on the Parker Solar Probe. *Astrophys J Suppl* 246(2):74. <https://doi.org/10.3847/1538-4365/ab7370>
- Wicks RT, Roberts DA, Mallet A, Schekochihin AA, Horbury TS, Chen CHK (2013) Correlations at large scales and the onset of turbulence in the fast solar wind. *Astrophys J* 778(2):177. <https://doi.org/10.1088/0004-637X/778/2/177>
- Wilson LB III, Stevens ML, Kasper JC, Klein KG, Maruca BA, Bale SD, Bowen TA, Pulupa MP, Salem CS (2018) The statistical properties of solar wind temperature parameters near 1 au. *Astrophys J Suppl Ser* 236:41. <https://doi.org/10.3847/1538-4365/aab71c>
- Wilson LB III, Brosius AL, Gopalswamy N, Nieves-Chinchilla T, Szabo A, Hurley K, Phan T, Kasper JC, Lugaz N, Richardson IG, Chen CHK, Verscharen D, Wicks RT, TenBarge JM (2021) A quarter century of wind spacecraft discoveries. *Rev Geophys* 59(2):e2020RG000714. <https://doi.org/10.1029/2020RG000714>
- Woodham LD, Wicks RT, Verscharen D, Owen CJ (2018) The role of proton cyclotron resonance as a dissipation mechanism in solar wind turbulence: a statistical study at ion-kinetic scales. *Astrophys J* 856(1):49. <https://doi.org/10.3847/1538-4357/aab03d>
- Woodham LD, Wicks RT, Verscharen D, TenBarge JM, Howes GG (2021) Dependence of solar wind proton temperature on the polarization properties of Alfvénic fluctuations at ion-kinetic scales. *Astrophys J* 912(2):101. <https://doi.org/10.3847/1538-4357/abed51>
- Wu P, Perri S, Osman K, Wan M, Matthaeus WH, Shay MA, Goldstein ML, Karimabadi H, Chapman S (2013) Intermittent heating in solar wind and kinetic simulations. *Astrophys J Lett* 763:30. <https://doi.org/10.1088/2041-8205/763/2/L30>
- Yang Y, Matthaeus WH, Parashar TN, Haggerty CC, Roytershteyn V, Daughton W, Wan M, Shi Y, Chen S (2017) Energy transfer, pressure tensor, and heating of kinetic plasma. *Phys Plasmas* 24(7):072306. <https://doi.org/10.1063/1.4990421>
- Yang Y, Wan M, Matthaeus WH, Sorriso-Valvo L, Parashar TN, Lu Q, Shi Y, Chen S (2019) Scale dependence of energy transfer in turbulent plasma. *Mon Not R Astron Soc* 482(4):4933–4940. <https://doi.org/10.1093/mnras/sty2977>
- Zank GP, Matthaeus WH (1992) The equations of reduced magnetohydrodynamics. *J Plasma Phys* 48:85–100. <https://doi.org/10.1017/S002237780001638X>
- Zank GP, Matthaeus WH, Smith CW (1996) Evolution of turbulent magnetic fluctuation power with heliospheric distance. *J Geophys Res* 101(A8):17093–17108. <https://doi.org/10.1029/96JA01275>
- Zhang L, He J, Narita Y, Feng X (2021) Reconstruction test of turbulence power spectra in 3D wavenumber space with at most 9 virtual spacecraft measurements. *J Geophys Res Space Phys* 126(1):27413. <https://doi.org/10.1029/2019JA027413>
- Zhao L-L, Zank GP, He JS, Telloni D, Hu Q, Li G, Nakanotani M, Adhikari L, Kilpua EKJ, Horbury TS, O'Brien H, Evans V, Angelini V (2021) Turbulence and wave transmission at an ICME-driven shock observed by the solar orbiter and wind. *Astron Astrophys* 656:3. <https://doi.org/10.1051/0004-6361/202140450>
- Zhuravleva I, Allen SW, Mantz A, Werner N (2018) Gas perturbations in the cool cores of galaxy clusters: effective equation of state, velocity power spectra, and turbulent heating. *Astrophys J* 865(1):53. <https://doi.org/10.3847/1538-4357/aadae3>
- Zweibel EG (2013) The microphysics and macrophysics of cosmic rays. *Phys Plasmas* 20(5):055501. <https://doi.org/10.1063/1.4807033>

Publisher's Note Springer Nature remains neutral with regard to jurisdictional claims in published maps and institutional affiliations.

Authors and Affiliations

Kristopher G. Klein¹  · Harlan Spence²  · Olga Alexandrova³  · Matthew Argall²  · Lev Arzamasskiy⁴  · Jay Bookbinder⁵ · Theodore Broeren¹  · Damiano Caprioli⁶  · Anthony Case⁷  · Benjamin Chandran²  · Li-Jen Chen⁸  · Ivan Dors²  · Jonathan Eastwood⁹  · Colin Forsyth¹⁰  · Antoinette Galvin²  · Vincent Genot¹¹  · Jasper Halekas¹²  · Michael Hesse⁵  · Butler Hine⁵ · Tim Horbury⁹  · Lan Jian⁸  · Justin Kasper⁷  · Matthieu Kretzschmar¹³  · Matthew Kunz¹⁴ 

Benoit Lavraud^{11,15}  · **Olivier Le Contel**¹⁶  · **Alfred Mallet**¹⁷  · **Bennett Maruca**¹⁸  · **William Matthaeus**¹⁸  · **Jonathan Niehof**²  · **Helen O'Brien**⁹  · **Christopher Owen**¹⁰  · **Alessandro Retinò**¹⁶  · **Christopher Reynolds**¹⁹  · **Owen Roberts**²⁰  · **Alexander Schekochihin**²¹  · **Ruth Skoug**²²  · **Charles Smith**²  · **Sonya Smith**² · **John Steinberg**²²  · **Michael Stevens**²³  · **Adam Szabo**⁸  · **Jason TenBarge**¹⁴  · **Roy Torbert**⁴  · **Bernard Vasquez**⁴  · **Daniel Verscharen**¹⁰  · **Phyllis Whittlesey**¹⁷  · **Brittany Wickizer**⁵ · **Gary Zank**²⁴  · **Ellen Zweibel**²⁵ 

✉ K.G. Klein
kgklein@arizona.edu

✉ H. Spence
harlan.spence@unh.edu

- 1 Lunar and Planetary Laboratory, University of Arizona, Tucson, AZ 85721, USA
- 2 Space Science Center, University of New Hampshire, Durham, NH 03824, USA
- 3 Observatoire de Paris, LESIA, Meudon, 92190, France
- 4 Institute for Advanced Study, Princeton, NJ 08540, USA
- 5 Ames Research Center, NASA, Mountain View, CA 94043, USA
- 6 Department of Astronomy & Astrophysics, University of Chicago, Chicago, IL 60637, USA
- 7 BWX Technologies, Inc., Washington, DC 20001, USA
- 8 Heliophysics Science Division, NASA Goddard Space Flight Center, Greenbelt, MD 20771, USA
- 9 Blackett Laboratory, Imperial College London, London, SW7 2AZ, UK
- 10 Mullard Space Science Laboratory, University College London, Dorking, RH5 6NT, UK
- 11 Institut de Recherche en Astrophysique et Planetologie, 31028 Toulouse, France
- 12 Department of Physics and Astronomy, University of Iowa, Iowa City, IA 52242, USA
- 13 Laboratoire de Physique et Chimie de l'Environnement et de l'Espace, CNRS and Université d'Orléans, 45071 Orléans, France
- 14 Department of Astrophysical Sciences, Princeton University, Princeton, NJ 08540 USA
- 15 Laboratoire d'astrophysique de Bordeaux, Univ. Bordeaux, CNRS, Pessac, France
- 16 Laboratoire de Physique des Plasmas, CNRS/Sorbonne Université/Université Paris-Saclay/Observatoire de Paris/Ecole Polytechnique Institut Polytechnique de Paris, Paris, 75005 France
- 17 Space Sciences Laboratory, University of California Berkeley, Berkeley, CA 94720, USA
- 18 Department of Physics & Astronomy, University of Delaware, Newark, DE 19716, USA
- 19 Institute of Astronomy, University of Cambridge, Cambridge, CB3 0HA, UK
- 20 Space Research Institute, Austrian Academy of Sciences, Graz, Austria
- 21 Rudolf Peierls Centre for Theoretical Physics, University of Oxford, Oxford, OX1 3PU, UK
- 22 Los Alamos National Laboratory, Las Alamos, NM 87545, USA
- 23 Center for Astrophysics, Harvard & Smithsonian, Cambridge, MA 02138, USA
- 24 Department of Space Science, University of Alabama in Huntsville, Huntsville, AL 35899, USA
- 25 Department of Astronomy, University of Wisconsin-Madison, Madison, WI 53706, USA